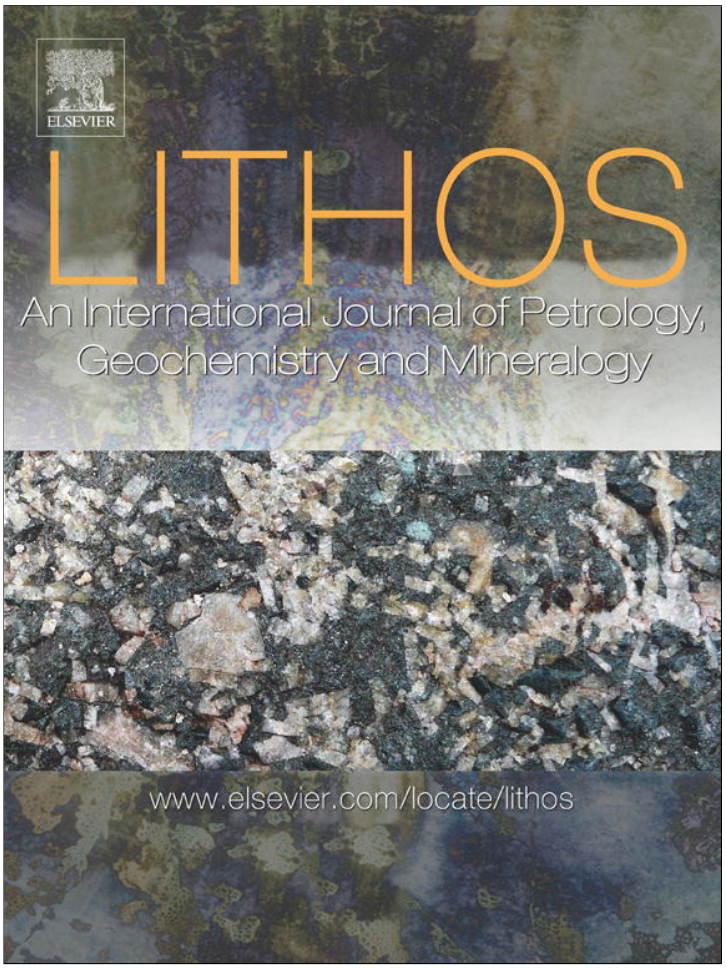

(This is a sample cover image for this issue. The actual cover is not yet available at this time.)

Lithos 168-169 (2013) 33–47

Contents lists available at SciVerse ScienceDirect

Lithos

journal homepage: www.elsevier.com/locate/lithos

Geochemistry and tectonic evolution of the Late Cretaceous Gogher–Baft ophiolite, central Iran

Hadi Shafaii Moghadam [a,*], Robert J. Stern [b], Massimo Chiaradia [c], Mohamad Rahgoshay [d]

[a] School of Earth Sciences, Damghan University, Damghan 36716-41167, Iran
[b] Geosciences Dept., University of Texas at Dallas, Richardson, TX 75083-0688, USA
[c] Département de Minéralogie, Université de Genève, Genève, Switzerland
[d] Faculty of Earth Sciences, Shahid Beheshti University, Tehran, Iran

ARTICLE INFO

Article history:
Received 16 October 2012
Accepted 21 January 2013
Available online 10 February 2013

Keywords:
Gogher–Baft ophiolite
Geochemistry
Subduction initiation
Supra-subduction zone
Neo-Tethys
Iran

ABSTRACT

The Late Cretaceous Gogher–Baft ophiolite is one of the best preserved remnants of Neo-Tethyan oceanic lithospheric within the inner Zagros ophiolite belt. The ophiolite comprises from bottom to top, harzburgites, pegmatite and isotropic gabbroic lenses within the mantle sequence, pillowed to massive basalts to dacites and pyroclastic rocks associated with blocks of pelagic limestone and radiolarite. Basaltic to dacitic sills cross-cut the pyroclastic rocks. The ophiolite sequence is overlain by Turonian–Maastrichtian pelagic limestones (93.5–65.5 Ma). Mineral compositions of harzburgites are similar to those of fore-arc peridotites and overlap with abyssal peridotites. Most Gogher–Baft ophiolite magmatic rocks show supra-subduction zone affinities, except for some E-MORB type lavas. The geochemical characteristics suggest that Gogher–Baft ophiolite magmatic rocks were generated during subduction initiation. These show progressive source depletion leading to the formation of MORB to boninitic magmas. Early E-MORB-type pillow lavas may have originated by melting mantle that was not affected by subduction components as the Tethyan oceanic plate began to sink beneath Eurasia as subduction began in the Late Cretaceous. Initial εNd (t) values range from +2.6 to +9 for Gogher–Baft magmatic rocks. Samples with radiogenic Nd overlap with least radiogenic MORBs and with Oman and other Late Cretaceous Tethyan ophiolitic rocks. The initial $^{87}Sr/^{86}Sr$ ratios range from 0.7048 to 0.7057, indicating modification due to seafloor alteration. Radiogenic $^{207}Pb/^{204}Pb$ isotopic compositions (systematically above the NHRL) and less radiogenic Nd isotopic compositions suggest the involvement of sediments in the mantle source in some magmatic rocks. Our results for Gogher–Baft ophiolite and the similarity of these to other Iranian Zagros ophiolites suggest a subduction initiation setting for the generation of these magmatic rocks.

1. Introduction

Ophiolites are relicts of oceanic lithosphere that commonly delineate suture zones between continental terranes. They are important markers of convergent margin processes and preserve the records of tectonic and magmatic events from rift-drift through subduction, accretion and collision stages of continental margin evolution (Dilek and Furnes, 2011). Ophiolites are interpreted to form in a wide variety of plate tectonic settings including oceanic spreading centers, back arc basins, fore arcs, as well as arc and other extensional settings including hotspots (Dilek et al., 2007; Kusky, 2004; Pearce and Robinson, 2010; Santosh et al., 2009; among others). Among the various categories of ophiolites, the mid-ocean ridge (MOR) and suprasubduction zone (SSZ) types constitute the major categories (Pearce et al., 1984).

The origin and tectonic evolution of ophiolites provide important constraints on the evolution of orogenic belts. Understanding ophiolites in a region such as Iran, the geologic history of which is dominated by accretionary tectonics where tectonostratigraphic terranes of different origin are now juxtaposed (Ghazi et al., 2003), is particularly important. The Zagros Orogenic Belt which formed by the most recent and ongoing accretion, reflects the Oligo-Miocene closure of Tethys. The growth of Zagros Orogenic Belt accompanies the continuing subduction of Arabia beneath Iran, with continental contact commencing at 10–20 Ma (McQuarrie et al., 2003). The abundant Zagros Orogenic Belt ophiolites thus define the evolving suture between Arabia and Eurasia.

The Zagros ophiolitic belt, of central interest to this study, lies along the NE flank of the Zagros fold-thrust belt and marks a Late Cretaceous episode of subduction initiation on the northern side of Neotethys (Shafaii Moghadam et al., 2010). Zagros ophiolites constitute the central parts of the Late Cretaceous Tethyan ophiolite belt, which extends ~3000 km from Cyprus to Oman (e.g., Alabaster et al., 1982; Dilek and Furnes, 2009; Dilek et al., 2007; Floyd et al., 1998; Garfunkel, 2006; Godard et al., 2003, 2006; Robertson and Mountrakis, 2006; Robertson, 1998, 2002; Sengor, 1990; among others). Although Zagros ophiolites make up almost half of the length of the Tethyan ophiolite belt, their

* Corresponding author. Tel./fax: +98 232 5235314.
E-mail address: hadishafaii@du.ac.ir (H.S. Moghadam).

0024-4937/$ – see front matter © 2013 Elsevier B.V. All rights reserved.
http://dx.doi.org/10.1016/j.lithos.2013.01.013

tectonic evolution is relatively poorly constrained due to limited field, geochemical and geochronological data. Zagros ophiolites can be subdivided into an "inner belt" and an "outer belt" south of the Main Zagros Thrust Fault and along the SW periphery of the Central Iranian block (Stocklin, 1977). Hereafter, we use "Outer Zagros Ophiolite Belt" and "Inner Zagros Ophiolitie Belt" for describing the two NW–SE belts containing the Neyriz-Haji-Abad and Nain -Gogher–Baft ophiolites, respectively (Fig. 1).

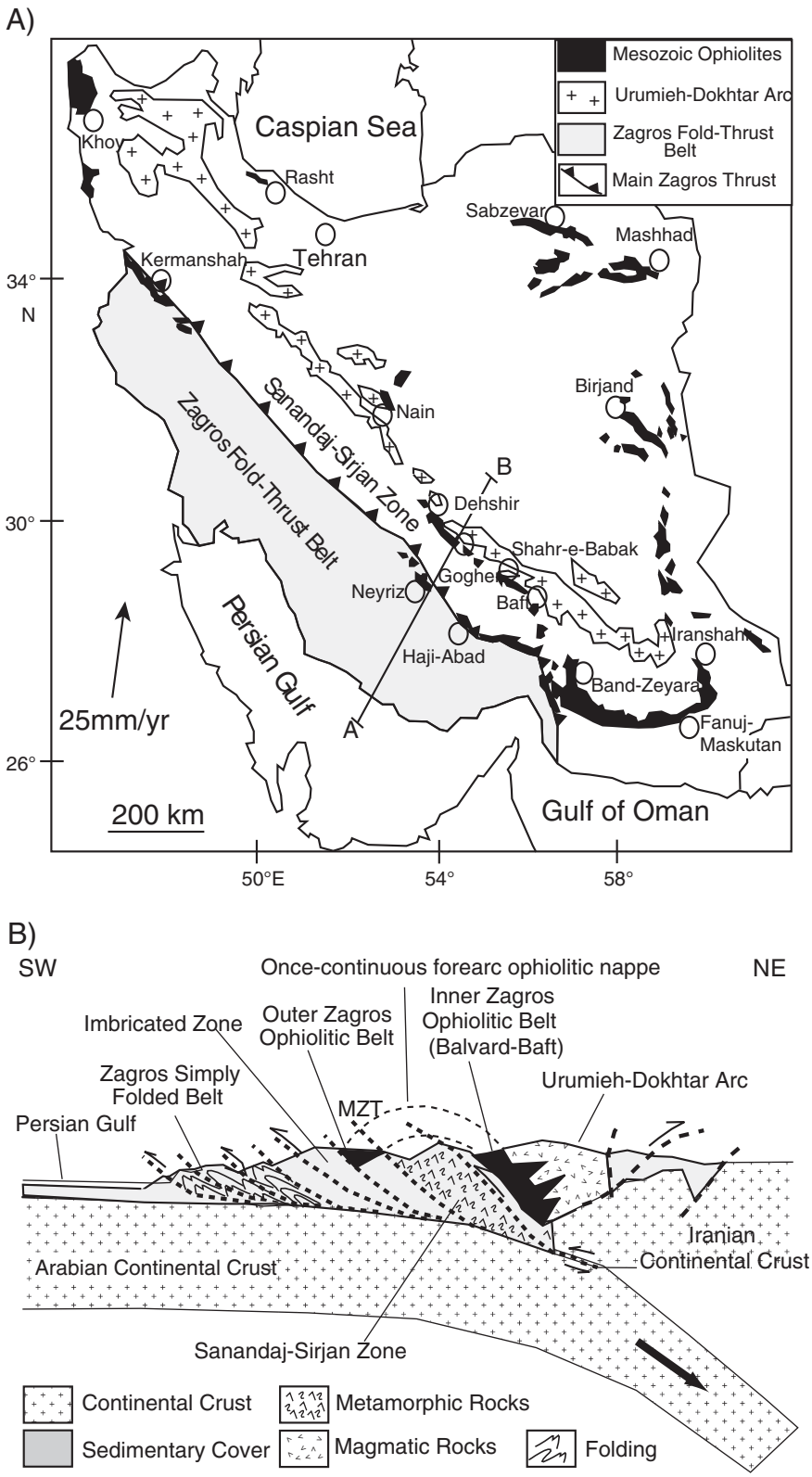

Fig. 1. (A) Map showing the distribution of the Nain-Baft (inner) Zagros ophiolitic belt, the Kermanshah-Neyriz-Haji-Abad (outer) Zagros ophiolitic belt, the location of the Urumieh–Dokhtar magmatic arc (Eocene-Quaternary), and the main Zagros thrust (MZT). (B) Schematic cross section showing the relations between the outer and the inner Zagros ophiolitic belts and the Zagros thrust-fold belt (after Shafaii Moghadam et al., 2010).

The Outer Zagros Ophiolitic Belt has been considered as slices of Tethyan oceanic lithosphere scraped off during NE-directed subduction underneath Iran (e.g., Babaie et al., 2001; Braud, 1970, 1978; Ricou, 1971, 1976; Ricou et al., 1977). The Inner Zagros Ophiolitic Belt is less well-known. The Inner Belt is described as ophiolitic mélange defining the SW margin of the Central Iranian block (e.g., Arvin and Robinson, 1994; Arvin and Shokri, 1996; Berberian and King, 1981; Davoudzadeh, 1972; Desmons and Beccaluva, 1983; McCall and Kidd, 1981; Stocklin et al., 1972). Inner Belt tectonic setting is controversial, and has been interpreted in several ways over the past four decades such as: (1) a narrow, Red Sea-like ocean, created at a slow spreading center (e.g., Babaie et al., 2001; Berberian and King, 1981; Davoudzadeh, 1972); (2) a Cretaceous arc basin related to Tethyan subduction that was inferred to have been active from upper Triassic to Miocene (e.g., Delaloye and Desmons, 1980; Ghazi and Hassanipak, 2000); (3) a Late Cretaceous back-arc basin (Agard et al., 2006; Shafaii Moghadam et al., 2009; Shahabpour, 2005); and (4) as part of a forearc that formed when subduction began beneath Southern Iran in Late Cretaceous time (Shafaii Moghadam and Stern, 2011; Shafaii Moghadam et al., 2010).

In this study we investigate the Gogher–Baft ophiolite complex, a typical Inner Belt ophiolite. This ophiolite was first studied by Dimitrijevic (1973) who carried out field mapping of the Kerman region. Here we report the first petrologic, geochemical, and isotopic study of this ophiolite. We use magmatic chemostratigraphy to trace the geochemical evolution of the ophiolite through time. A previous report, on the Dehshir ophiolite (Shafaii Moghadam et al., 2010), applied the subduction initiation model of Stern and Bloomer (1992) to explain the formation of this and other Late Cretaceous Inner and Outer Belt ophiolites. In this contribution, we report the field characteristics, mineral chemistry, whole rock geochemistry as well Sr–Nd–Pb isotope data to evaluate the petrogenesis of Gogher–Baft ophiolitic rocks.

2. Field observations

The Gogher–Baft ophiolite occurs as a 5–10 km wide and about 60 km long, WNW-trending belt. The ophiolite is composed of ultramafic and mafic rocks, capped by Turonian–Maastrichtian (93.5–65.5 Ma) pelagic sediments resting directly on the ophiolite (Figs. 2, 3). Gogher–Baft is a dismembered ophiolite, and does not contain ultramafic cumulates; cumulate gabbros, crustal isotropic gabbros or a sheeted dyke complex. Two types of basaltic pillow lavas and lava flows are recognized in the Baft and Gogher regions (Arvin and Robinson, 1994; Arvin and Shokri, 1996): 1 — tholeiitic basalts similar to N-MORB and 2 — transitional basalts, geochemically intermediate between MORB and island-arc tholeiites (IAT), the latter generated by melting of a subduction-modified mantle source.

Depleted harzburgite with abundant diabase dikes (Appendix 1B) constitute the ophiolite mantle sequence (Fig. 2). Isolated pockets of pegmatitic gabbro and lenses of isotropic gabbro occur in the upper mantle section. Isotropic gabbros are locally intruded by late diabasic, gabbroic and plagiogranitic dikes, especially N–NW of Baft town (Fig. 2). Podiform chromitites are hosted in mantle depleted harzburgites although they are typically enveloped by dunite. They are mainly pod-like and/or lensoid in form. The contact between the chromitite pods and host dunites or harzburgites is usually sharp.

A variety of Gogher–Baft volcanic rocks are found as tectonic slices: massive and pillowed basalt to andesite–dacite lava flows, showing faulted contacts with pelagic limestones and/or serpentinites (Appendix 1C). Hyaloclastites, cold breccias and pillow breccias are locally found throughout the volcanic pile.

Pyroclastic rocks including tuffs and volcanic breccias associated with blocks of pelagic limestone and radiolarite are common in the upper parts of this ophiolite. Pyroclastics constitute a 300–400 meter thick unit resting on ophiolitic basaltic flows (Fig. 3) and/or pillow

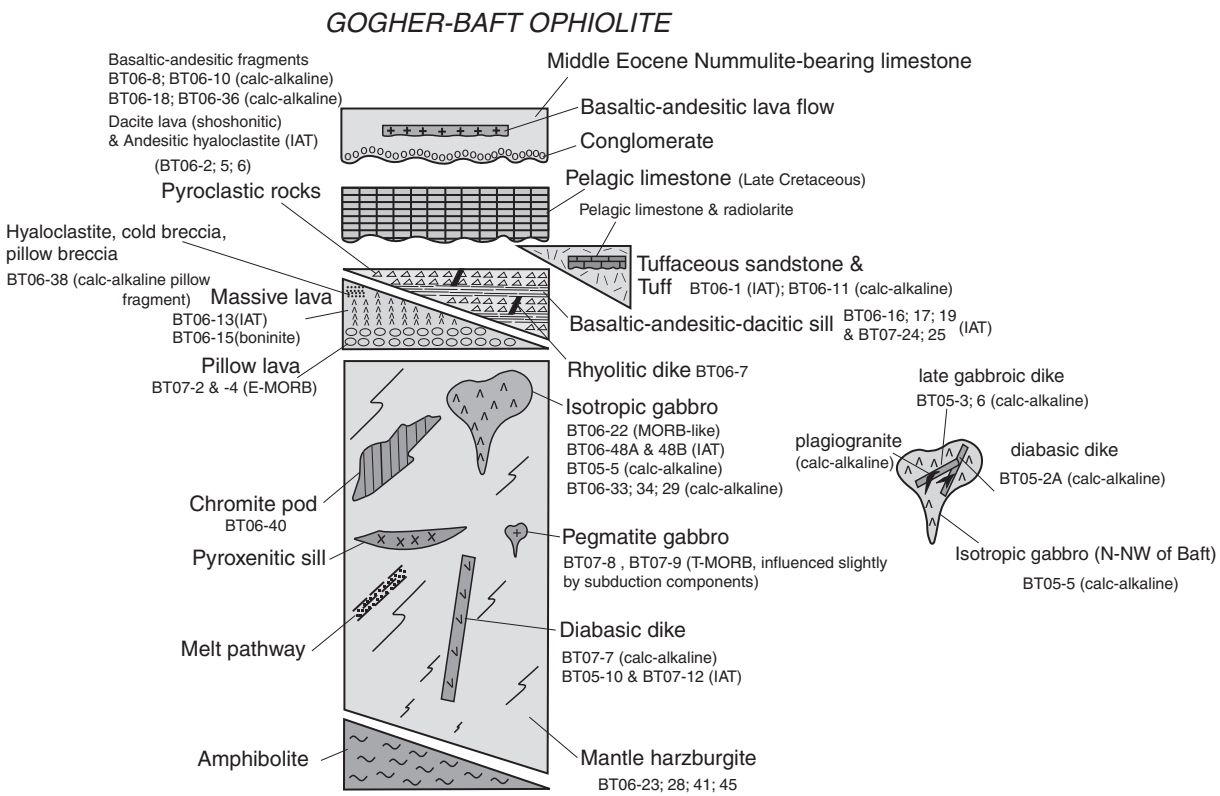

Fig. 2. Simplified stratigraphic column illustrating the idealized internal lithologic successions in the Gogher–Baft ophiolite. The approximate stratigraphic positions of samples are also shown.

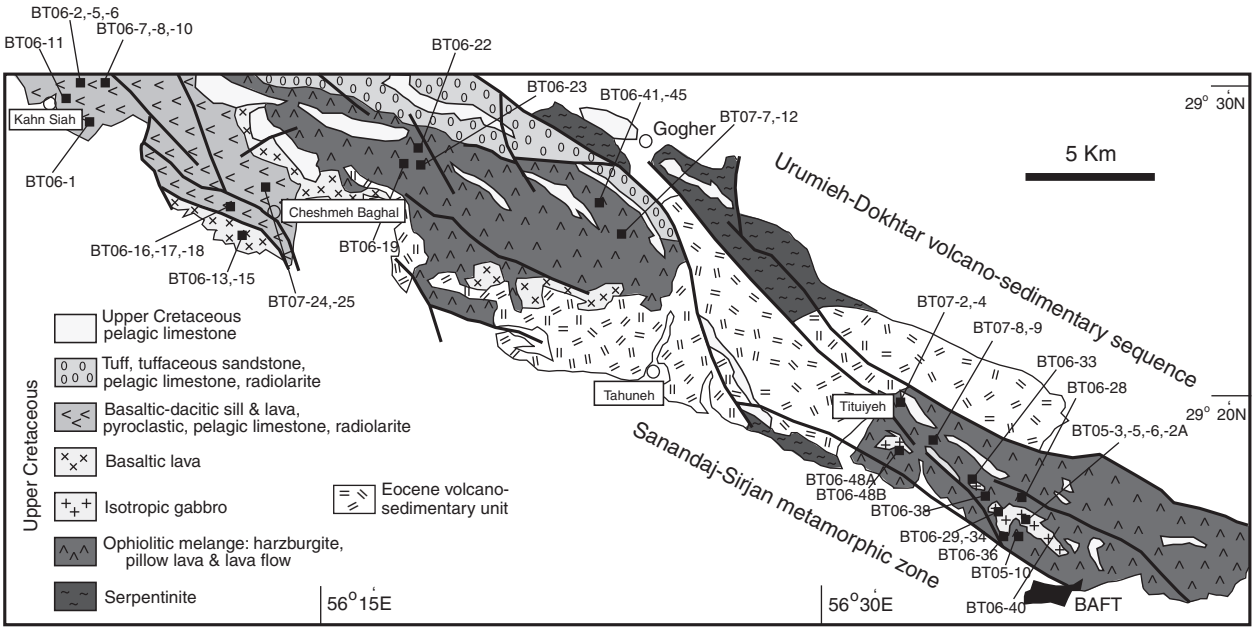

Fig. 3. Simplified geological map of the Gogher–Baft ophiolite (compiled after Mijalkovic et al., 1972; Srdic et al., 1972). Location of samples is also shown.

lavas (Mijalkovic et al., 1972). Pyroclastic rocks include volcanic breccias, agglomerates, tuff, tuffaceous sandstones and lutites, cold pillow breccias and andesitic hyaloclastites with basaltic–andesitic pillow fragments. Pyroclastic rocks are usually coarse in the SE and grade into finer-grained tuffs to the NW, suggesting that Late Cretaceous explosive volcanic centers — probably a nascent arc — existed east of the study area. Small andesitic-dacitic lava outcrops are also observed in the pyroclastics. Basaltic–andesitic and dacitic sills are common among the pyroclastic rocks (Appendix 1D, E). Rock fragments in the pyroclastic units range in composition from basalt (aphyric to pyroxene-phyric) to porphyritic or sanukitoid andesite. Rare rhyolitic dikes crosscut the pyroclastic rocks. At the top of the pyroclastic unit, thick sequences of tuff and tuffaceous sandstones with intercalated pelagic limestone and radiolarite are found along the northeast flank of the ophiolite (Fig. 3), in places with sedimentary contacts. The thickness of the pyroclastic unit increases to the NE, further suggesting that explosive arc volcanoes lay in that direction in Late Cretaceous time. This observation supports the hypothesis that the Gogher–Baft ophiolite and other massifs in the inner ophiolite belt represent a forearc to what subsequently became the Urumieh–Dokhtar magmatic arc.

Turonian–Maastrichtian limestones rest stratigraphically above the pyroclastic rocks, tuffaceous sandstones and/or the lavas (Appendix 1A).

3. Lithologic descriptions and mineral compositions

The locations of samples that were investigated in this study are shown stratigraphically in Fig. 2 and geographically in Fig. 3. About 80 thin sections from all rock units of the Gogher–Baft ophiolite were examined. From these, nine representative samples were selected for microprobe analyses, including podiform chromitite (BT06-40), harzburgites (BT06-28, BT06-41, and BT06-45), pegmatite gabbro (BT07-8), isotropic gabbro (BT06-22), andesitic fragment in breccia (BT06-10), basaltic and dacitic rocks (BT06-15, BT06-6) (see Appendix 3 for analytical methods).

3.1. Mantle sequence

This includes clinopyroxene-poor and clinopyroxene-free spinel harzburgites. Most of these rocks have been serpentinized, usually more than 60%, even up to 100%. Where the primary texture is preserved, the harzburgite shows porphyroclastic nature, with coarse, deformed orthopyroxene grains (generally 1–3 mm, max. 5 mm) (Appendix 2A).

Relict olivines are homogenous, ranging in composition from Fo_{90} to Fo_{92}, indicating that the harzburgite is moderately depleted. Olivine NiO contents vary between 0.29 and 0.54 wt.% (Appendix 6). Orthopyroxene porphyroclasts in harzburgite have compositions ranging between $Wo_6En_{85}Fs_9$ and $Wo_2En_{91}Fs_7$. Their Mg# ($Mg/Mg+Fe^{2+}$) ranges from 0.90 to 0.93 (Appendix 7). Orthopyroxenes contain relatively low Al_2O_3 (2.2–3.7%) and Cr_2O_3 (0.4–1.1%) contents (Appendix 7) (Fig. 4A).

Gogher–Baft harzburgite contains diopsidic clinopyroxene. The Mg# of clinopyroxene cores ranges from 92.1 to 94.2 (Appendix 7). Al_2O_3 and TiO_2 contents are markedly low, similar to clinopyroxenes from depleted fore-arc harzburgites (Ishii et al., 1992), and comparable to those from other inner and outer belt harzburgites (Fig. 4B & Appendix 7).

Spinel in the Gogher–Baft harzburgite is dark brown, with Mg# ($Mg/Mg+Fe^{+2+}$) varying between 0.57 and 0.76. The Cr# value ($Cr/Cr+Al$) of harzburgite spinel cores ranges between 0.45 and 0.53 (Appendix 8). Podiform chromitites have higher Cr#, between 0.84 and 0.85. As shown in Fig. 5A, the high Cr# of the Baft–Gogher harzburgite spinels plots in the compositional range defined by spinels from both fore-arc harzburgites and depleted abyssal peridotites (Dick and Bullen, 1984). Podiform chromitites plot in the boninitic field (Fig. 5A). The TiO_2 content of harzburgite spinels is less than 0.1 wt.%, similar to those from fore-arc harzburgites as reported by Tamura and Arai (2006) (Fig. 5B). TiO_2 content of chromitites is less than about 0.2 wt.%.

3.2. Pegmatite gabbros

Gogher–Baft ophiolite pegmatite gabbros occur as small pockets within the mantle harzburgite. Plagioclase and clinopyroxene are the predominant rock-forming phases, whereas olivine and spinel occur as trace phases (<3%). Two types of plagioclase can be distinguished: a coarse, slightly zoned variety and a fine-grained variety occurring interstitially between large plagioclase and clinopyroxene phenocrysts. Pegmatite gabbros have olivine with Fo_{83} and 0.25 to 0.30% NiO (Appendix 6).

Clinopyroxene in pegmatite gabbros is diopside to augite, with low Al_2O_3 and TiO_2 and high Mg# and Cr_2O_3 content (Appendix 9), indicating crystallization from a primitive melt (De Bari and Coleman, 1989).

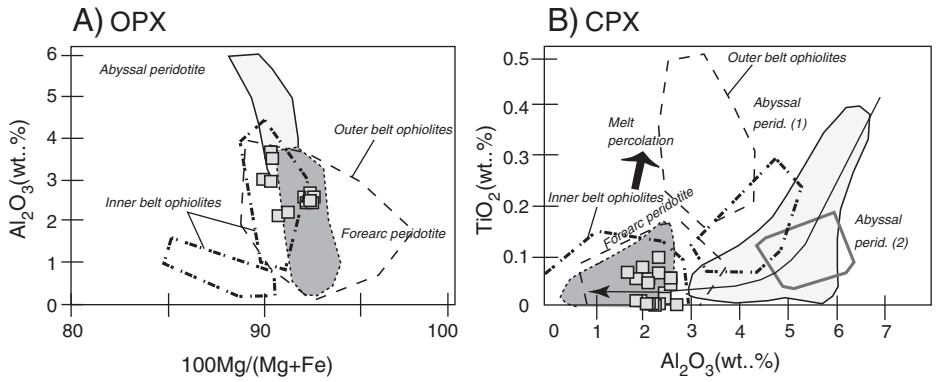

Fig. 4. (A) Al_2O_3 vs. Mg# variations of orthopyroxene in harzburgite from the Gogher–Baft ophiolite. Fields for abyssal peridotites (Johnson et al., 1990) and forearc peridotites (Ishii et al., 1992) are shown for comparison. (B) TiO_2 vs. Al_2O_3 composition of clinopyroxene in harzburgite from the Gogher–Baft harzburgite. Comparative fields are shown for abyssal peridotites (Abyssal peridotite 1; Hébert et al., 1990); (Abyssal peridotite 2; Johnson et al., 1990) and fore-arc peridotite (Ishii et al., 1992). The long, thin arrow shows changes expected for residual clinopyroxene due to progressive partial melting of peridotite. Short thick arrow shows compositional changes due to re-equilibration of Clinopyroxene with percolating melt. For comparison, we also show fields for inner Zagros (data from Shafaii Moghadam, 2009) and outer Zagros ophiolitic belts (data from Shafaii Moghadam et al., 2012b for Haji-Abad ophiolite; unpublished data for Kermanshah and Neyriz ophiolites).

Fine-grained plagioclases are andesine and coarse plagioclases are bytownite (Appendix 10).

3.3. Mafic-intermediate magmatic rocks

Gogher–Baft ophiolite mafic igneous rocks include isotropic gabbros, pillow lavas, basaltic–andesitic flows, basaltic–andesitic sills in pyroclastic rocks and diabasic dikes intruding harzburgite and/or isotropic gabbro. Plagioclase and clinopyroxene are the main constituents of the isotropic gabbros (Appendix 2B). In more hydrothermally altered samples (dioritic facies), green amphibole (actinolite) and highly altered plagioclase dominate (Appendix 2C). Clinopyroxenes are Fe-rich augite, with Mg# and TiO_2 ranging from 67.4 to 69.7 and 0.57 to 0.95% respectively (Appendix 9).

Ophiolitic lavas are porphyritic, with coarse-grained, euhedral to subhedral plagioclase (1 to >4 mm) and subhedral to anhedral clinopyroxene (2–3 mm) phenocrysts in an altered glassy groundmass with plagioclase microlites (Appendix 2D). Clinopyroxene in basaltic lavas is high-Mg augite and diopside, with higher Mg# and lower TiO_2 compared to those of isotropic gabbros (Appendix 9).

Andesitic and dacitic lavas are characterized by plagioclase phenocrysts (>1–2 mm) and microlites (<0.2 mm). Coarse-grained plagioclase can be subdivided into two groups: euhedral to subhedral phenocrysts with relatively uniform labradorite (An_{51-57}) cores (Appendix 9) and corroded phenocrysts (composition not measured) suggesting disequilibrium. Hornblende in the andesite shows oxidized margins and alteration into chlorite and clays (Appendix 2E).

Basaltic–andesitic and dacitic sills in pyroclastic rocks include highly altered plagioclase laths set in a groundmass of altered glass and plagioclase microlites. Clinopyroxene phenocrysts (1–1.5 mm) are present, except in the dacites.

Diabasic dikes intrude mantle harzburgite and isotropic gabbros (associated with microgabbro dikes; see Fig. 2). These diabasic dikes include saussuritized plagioclase microlites associated with chloritized–uralitized clinopyroxene.

3.4. Pyroclastic rocks and hyaloclastites

Volcanic breccias, agglomerates and hyaloclastites are characterized by angular volcanic rock fragments in a groundmass of clays,

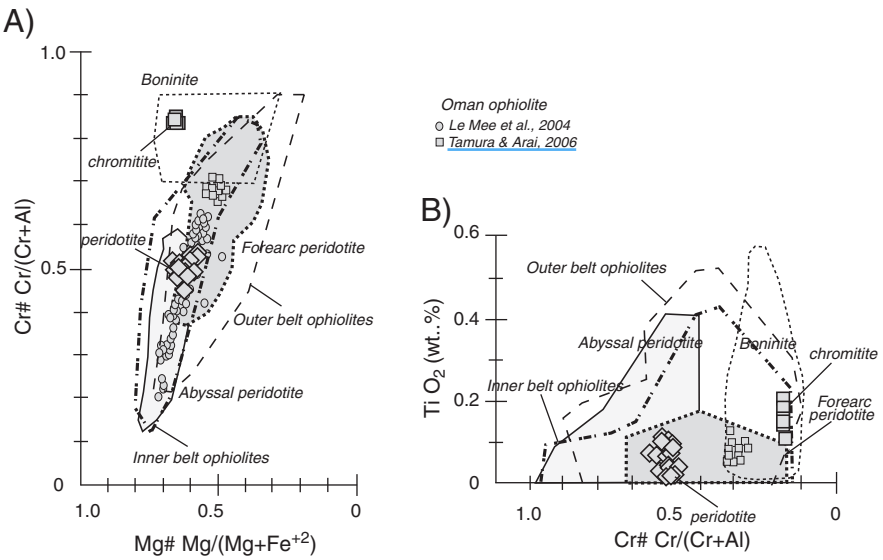

Fig. 5. (A) Cr# vs. Mg# diagram (modified after Dick and Bullen, 1984) for spinels in harzburgite from the ophiolite suite. (B) Diagram (after Tamura and Arai, 2006) showing TiO_2 against Cr# of spinels, in order to discriminate between various types of peridotites and link to boninite. Note that spinels plot in the fields for both fore-arc peridotites and boninites. For comparison, we also show fields for inner Zagros (data from Shafaii Moghadam, 2009) and outer Zagros ophiolitic belts (data from Shafaii Moghadam et al., 2012b for Haji-Abad ophiolite; unpublished data for Kermanshah and Neyriz ophiolites). Oman harzburgite spinel data are from Le Mée et al. (2004) and Tamura and Arai (2006).

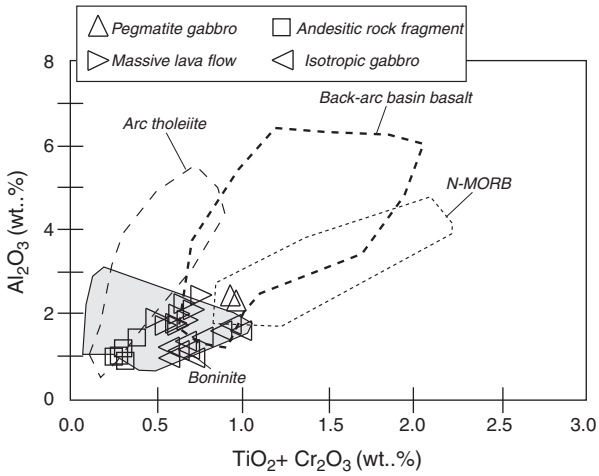

Fig. 6. Compositional variations of clinopyroxene from different magmatic rocks of the Gogher–Baft ophiolite in Al_2O_3 vs. $TiO_2+Cr_2O_3$ diagram (adapted after Hout et al., 2002). Fields outline clinopyroxene compositions in boninites (VanderLaan et al., 1992), island-arc tholeiites and back-arc basin basalts (Hawkins and Allan, 1994), and N-MORB (Stakes and Franklin, 1994).

polycrystalline fine-grained quartz, and chlorite. Broken and angular plagioclase and quartz are also present between rock fragments (Appendix 2H). Pyroclastic rock fragments are divided into basaltic, andesitic and sanukitoids. The basaltic–andesitic fragments contain large clinopyroxene and plagioclase phenocrysts.

Orthopyroxene phenocrysts (0.5–2 mm) are common in the sanukitoid rock fragments (Appendix 2F). The sanukitoids contain plagioclase phenocrysts (0.5–2 mm) with oscillatory and/or patchy zoning and sieve texture confirming either rapid decompression or magma mixing (Nelson and Montana, 1992) (Appendix 2G). Some plagioclase phenocrysts show complex zoning between core and rim.

Clinopyroxene in the andesitic fragments is augite with higher Fe content than that in basalt. The Mg#, Al_2O_3 and TiO_2 in clinopyroxene vary from 71.4 to 73.3, 0.95 to 1.4% and 0.28 to 0.33% respectively (Appendix 9). Orthopyroxene phenocrysts are hypersthene to pigeonite and also show high Al_2O_3 content and low Mg# (Appendix 9). TiO_2 ranges between 0.2 and 0.4% (Appendix 9). Plagioclase in andesitic fragments is zoned between An_{41} and An_{91} (Appendix 10).

3.5. Clinopyroxene composition of mafic magmatic rocks

The composition of clinopyroxene in basaltic rocks provides a useful indicator of the different magma compositions and is therefore a good index to characterize the tectonic settings (Leterrier et al., 1982) as well as to classify the different ophiolite types (Hout et al., 2002). For this purpose, we applied the Al_2O_3 vs. $Cr_2O_3+TiO_2$ diagram of Hout et al. (2002) to clinopyroxenes from different Gogher–Baft ophiolite mafic-intermediate rock units (Fig. 6). These clinopyroxenes have low TiO_2 and Al_2O_3 and are mostly similar to clinopyroxenes in boninites (Fig. 6), excepting clinopyroxenes from the pegmatite gabbros, which are MORB-like. Low TiO_2 content of Gogher–Baft clinopyroxenes indicates a depleted mantle source (e.g., Pearce and Norry, 1979) and formation in a supra-subduction zone environment. MORB-like pegmatite gabbros perhaps reflect an early melt, produced during initial stage of subduction initiation and trapped as a lens within mantle peridotites.

4. Major, trace, REE and Sr–Nd–Pb isotope geochemistry

We present major and trace (REE) elements data for 39 whole rock samples including four harzburgites, two pegmatite gabbros, seven isotropic gabbros, two gabbroic dikes that intrude isotropic gabbros, four pillowed and flow basalts, nine pyroclastic rock fragments, seven samples of mafic–felsic sill and dikes within pyroclastic rocks and four samples of diabasic dikes that intrude harzburgite (Appendix 4). Sample positions and locations are shown in Figs. 2 and 3. The analyzed samples are characterized by variable loss on ignition (LOI; 1–8.2% except in peridotites with 1.6–10.9%). Because of the mobility of large ion lithophile elements (LILE) during alteration, we use immobile trace elements such as Rare Earth (REE) and high field strength elements (HFSE) to evaluate the geochemical signature and tectono-magmatic setting of these rocks. Selected rock samples (7 samples) were also investigated for their Sr, Nd and Pb isotopic compositions (Table 1).

4.1. Mantle sequence

4.1.1. Harzburgite

Gogher–Baft harzburgites are distinguished by Mg# ranging from 88.8 to 91.2. They have <1.3 wt.% Al_2O_3 and <1.00 wt.% CaO (Appendix 4) except for sample BT06-45, with 2.5 wt.% Al_2O_3 and 2.2 wt.% CaO.

Table 1
Sr–Nd–Pb isotopes composition of the Gogher–Baft ophiolitic rocks.

Sample	BT-06-7	BT-06-10	BT-06-19	BT-06-33	BT-07-4	BT-07-7	BT-07-12
Lithology	Rhyolitic dike	And. Fragment	Basaltic sill	Isotropic gab.	Pillow lava	Diabasic dike	Diabasic dike
Nd (ppm)	7.213	12.640	5.606	7.053	25.355	4.770	2.380
Sm (ppm)	2.747	2.922	2.002	2.178	6.070	1.487	0.919
Rb (ppm)	0.916	9.845	11.435	10.376	5.254	0.075	18.252
Sr (ppm)	102.924	660.615	212.166	360.812	225.169	38.526	138.302
U (ppm)	0.242	0.885	0.183	0.166	0.903	0.201	0.074
Th (ppm)	0.439	3.039	0.169	0.643	2.782	0.598	0.348
Pb (ppm)	0.452	11.758	0.564	0.671	1.605	0.463	0.842
$^{143}Nd/^{144}Nd$	0.5130325	0.5130204	0.5129630	0.5130190	0.5129242	0.5127630	0.5131228
2σ	0.0000011	0.0001806	0.0000024	0.0000017	0.0000014	0.0000014	0.0000037
$^{147}Sm/^{144}Nd$	0.2292545	0.1391693	0.2149731	0.1859616	0.1441348	0.1876849	0.2325661
$^{143}Nd/^{144}Ndi$	0.5128825	0.5129293	0.5128223	0.5128974	0.5128299	0.5126402	0.5129707
εNd (100 Ma)	7.28	8.20	6.11	7.57	6.26	2.55	9.00
$^{87}Sr/^{86}Sr$	0.7054312	0.7055535	0.7050837	0.7059087	0.7052499	0.7052382	0.7057374
2σ	0.0000028	0.0000051	0.0000029	0.0000108	0.0000053	0.0000017	0.0000067
$^{87}Rb/^{86}Sr$	0.0257321	0.0431071	0.1558950	0.0831849	0.0674957	0.0056536	0.3817448
$^{87}Sr/^{86}Sri$	0.7053946	0.7054923	0.7048622	0.7057905	0.7051540	0.7052302	0.7051950
$^{206}Pb/^{204}Pb$	19.0244068	18.4082445	18.1923617	19.1153838	19.0957275	18.9466563	18.5894309
$^{207}Pb/^{204}Pb$	15.6106058	15.5590351	15.5166269	15.6120822	15.5672758	15.6613230	15.6199890
$^{208}Pb/^{204}Pb$	38.8154508	38.4308986	38.1624197	39.2294819	39.1101426	39.0345090	38.6028173
$^{206}Pb/^{204}Pbi$	18.4860804	18.3336366	17.8725678	18.8650563	18.5273557	18.5097491	18.5017536
$^{207}Pb/^{204}Pbi$	15.5847582	15.5554528	15.5012720	15.6000628	15.5399856	15.6403449	15.6157792
$^{208}Pb/^{204}Pbi$	38.4946815	38.3468725	38.0654521	38.9113888	38.5359406	38.6072331	38.4678175

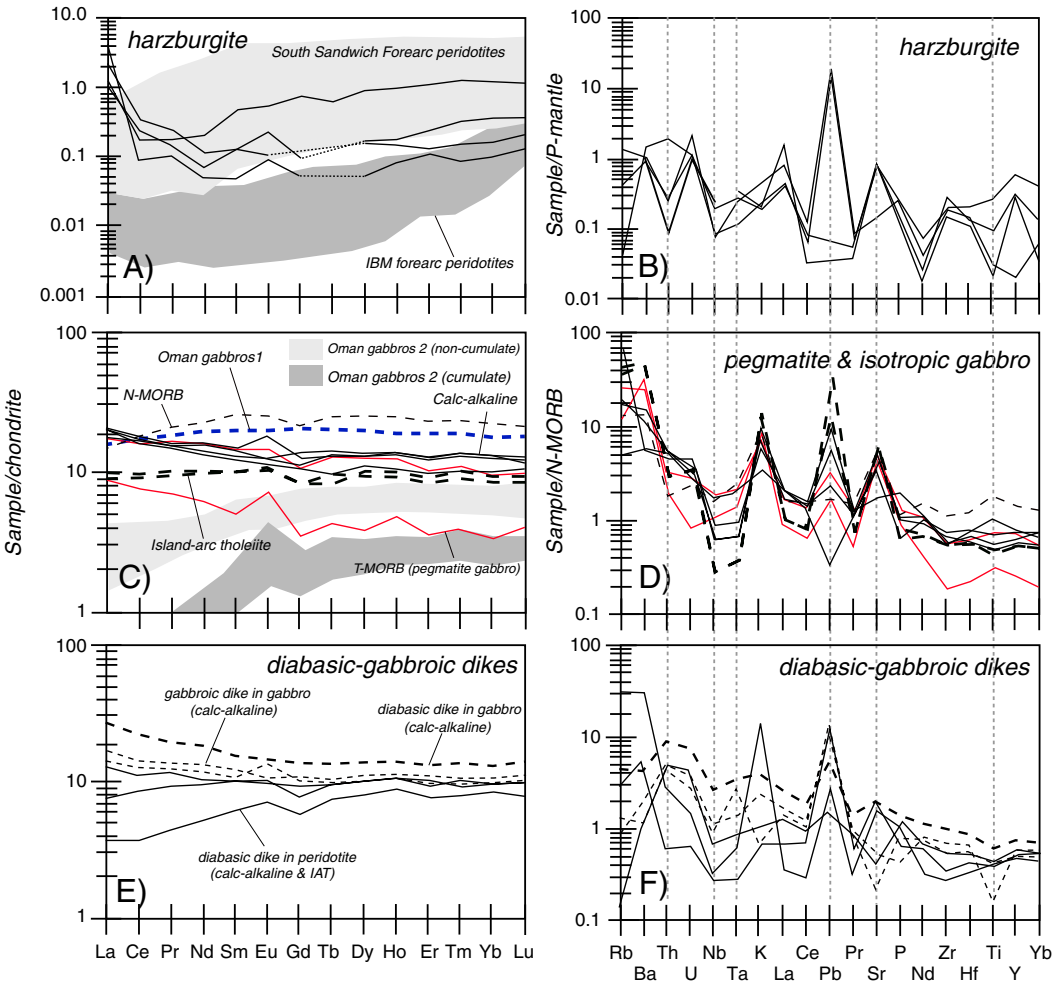

Fig. 7. Chondrite-normalized REE patterns (chondrite abundances from McDonough and Sun, 1995) and N-MORB normalized multi-elements patterns (N-MORB concentrations from Sun and McDonough, 1989) for rock units of the Gogher–Baft ophiolite. Mantle harzburgite trace elements are normalized relative to primary mantle (colored figure for online version).

REE abundances in harzburgites are low and show light REE enrichment and U-shape patterns, again excepting sample BT06-45 (Fig. 7A) with slightly enriched bulk REE content. Such selective LREE enrichment suggests interaction with trapped LREE-enriched melt or aqueous fluids, either liberated from the subducted slab or due to alteration during serpentinization (Bodinier et al., 1990; Gruau et al., 1998; Prinzhofer and Allègre, 1985). Alteration may be responsible for La enrichment as indicated by high LOI content of peridotites. LREE enrichment in whole rocks is also reported from abyssal peridotites (Niu, 2004). Nearly flat to upward-sloping MREE to HREE profiles indicate significant melt depletion, similar to South Sandwich Trench-Fracture Zone Intersection fore-arc harzburgite (Pearce et al., 2000) but clearly different from highly depleted Izu-Bonin–Mariana forearc peridotites. Sample BT06-45 is less refractory, as testified by the higher REE content with HREE enrichment (Fig. 7A) This sample might be a simple residue after relatively low-degrees of partial melting, although it might have been re-enriched by melt infiltration (Pearce et al., 2000).

LILE such as K, Rb, and Ba, which are sensitive to low-temperature alteration, do not show large positive anomalies, except for Pb and Sr (Fig. 7B).

4.1.2. Pegmatite gabbro

Pegmatite gabbros are characterized by variable Mg#, CaO, Al_2O_3 and CaO/Al_2O_3 ratio (Appendix 4). These have high bulk REE (Fig. 7C), with La = 8.9–17.6 × chondrite and Yb = 3.5–9.7 × chondrite. Sample BT07-8 is highly enriched. The pegmatite gabbros are in general slightly enriched in LREE (La/Yb = 1.8–2.6 × chondrite), with REE patterns similar to those of the Gogher–Baft ophiolitic basalts (see next section). There are no conspicuous Eu anomalies (except sample BT07-9 with slight Eu positive anomalies). The N-MORB normalized trace element patterns for pegmatite gabbros (Fig. 7D) reflect selective enrichment in highly incompatible elements (e.g., Rb, Ba and K) relative to LREE (e.g., Ba/La = 18.4–28.8 × N-MORB). They also show spikes in Sr and Pb (Sr/La = 2.7–5.2 × N-MORB and Pb/La = 1.8–1.9 × N-MORB) (Fig 7D). Gogher–Baft pegmatite gabbros do not show depletion in Nb and Ta relative to LREE (Nb/La = 1.1–1.2 × N-MORB). Such behavior along with slight enrichment in LREE relative to HREE is consistent with a T-MORB affinity, influenced by subduction components.

4.1.3. Isotropic gabbros

SiO_2 abundances in isotropic gabbros are variable (42.4–52.4 wt.%) and the lowest value (sample BT06-29, 42.4 wt.% SiO_2) is associated with high LOI and Na_2O contents (Appendix 4). The Al_2O_3 and Sc contents show only limited variations (Appendix 4) which differs from variations in the cumulate gabbros. The Mg#, TiO_2 and Zr contents of the isotropic gabbros are variable (Appendix 4). In the Ti/V diagram of Shervais (1982) (Fig 8), isotropic gabbros plot in IAT, boninite and MORB fields.

Gogher–Baft isotropic gabbros comprise three groups: (1) IAT-like gabbros (BT06-48A and BT06-48B) with flat REE patterns (Fig. 7C; e.g., La/Yb = 1.13–1.15 × chondrite), depletion in HFSE (Nb, Ta, Ti) and enrichment in LILEs (Ba, Rb, Th, K, Sr, Pb and U) relative to N-MORB (Fig. 7D); (2) calc-alkaline gabbros (BT06-29, BT06-33, BT05-5 and BT06-34) showing greater LREE enrichment (Fig. 7C).

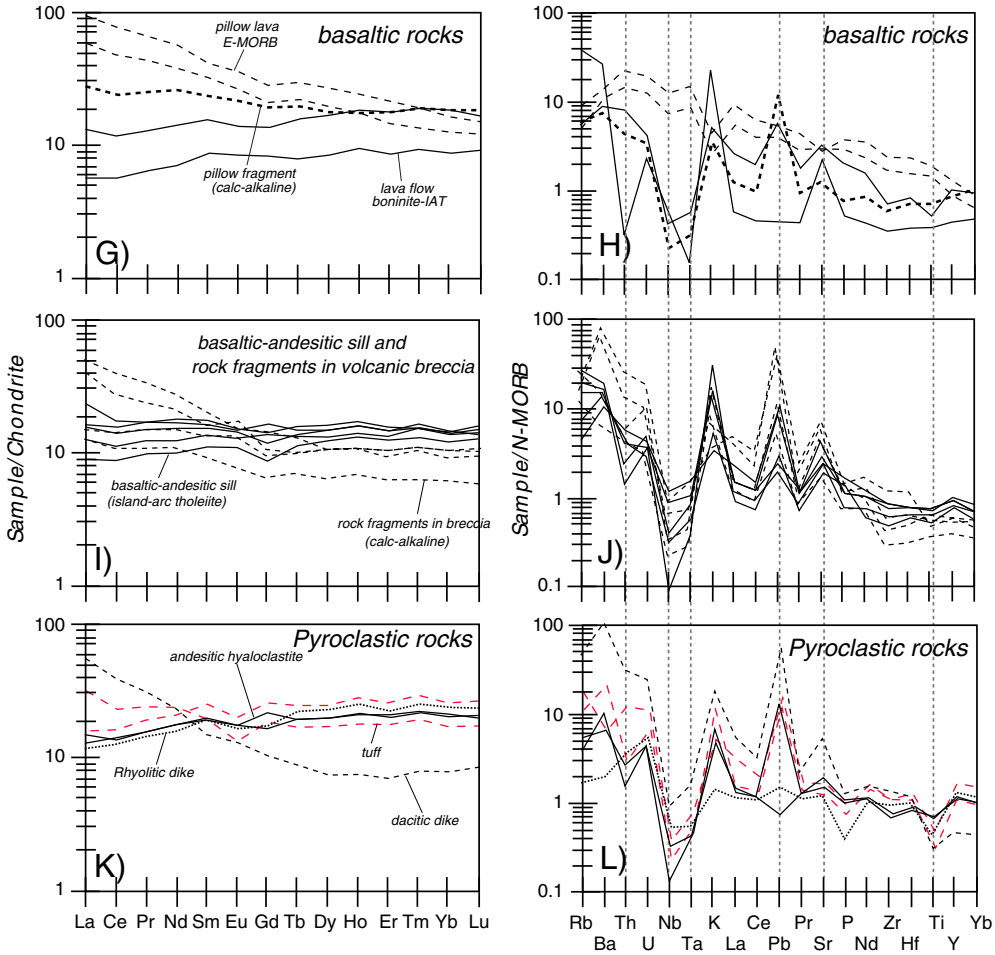

Fig. 7 (*continued*).

These samples also show enriched LILEs (Rb, Ba, Th, U, K, Pb) (except BT06-34), and Sr and depleted HFSE (Nb and Ta) relative to LREE (Fig. 6D); and (3) one MORB-like sample (BT06-22) showing LREE depletion (Fig. 7D; e.g., La/Yb = 0.7 × chondrite). Sample BT06-22 does not show Nb depletion relative to LREE and is geochemically similar to fractionated N-MORBs.

Gogher–Baft gabbros, both pegmatite and isotropic varieties, are geochemically different from Oman gabbros (Fig. 7C), except for MORB-like sample BT06-22, which is similar to Oman massive gabbros 1. Oman massive gabbros 1 show flat REE patterns, resembling N-MORBs (similar to the V1 lava unit) and are thought to have formed via partial melting o f residual MORB mantle, whereas massive (cumulate and non-cumulate) gabbros2 are suggested to form from residual mantle that was metasomatized by subduction components, similar to Oman V2 lavas (Tsuchiya et al., 2013).

4.1.4. Mafic dikes

Diabasic and gabbroic dikes intrude both mantle harzburgite (BT05-10, BT07-7 and BT07-12) and isotropic gabbro (BT05-2A, BT05-3 and BT05-6). The dikes show a broad range in silica content (40.3–52.7 wt.% SiO_2) with low values found in samples with high LOI and CaO due to calcite alteration. All other major elements except FeO seem to be diluted by high CaO. The dikes are primitive to fractionated (Mg# = 46–72) and contain variable TiO_2, Zr and Ti/V (Appendix 4). These fall into the IAT field of Shervais (1982) while gabbroic dike BT05-3 shows boninitic affinities with low abundances of Zr and TiO_2, low Ti/V and higher Mg# (Fig. 8, Appendix 3).

Diabasic dikes intruding harzburgites display slight LREE enrichment (e.g., La/Yb = 1.42 × chondrite, sample BT07-7; Fig. 7E) and/or LREE depletion (e.g., La/Yb = 0.8-0.5 × chondrite). Negative Nb and Ta anomalies and positive anomalies in Ba, Th, U, Pb, Sr, K characterize these diabasic dikes, similar to calc-alkaline/IAT series (Fig. 7F).

Diabasic dikes intruding isotropic gabbros are enriched in LREE relative to HREE (Fig. 7E). Relative to N-MORB, these dikes are enriched in Ba, Th, U, Pb and depleted in Nb and Ta, similar to calc-alkaline magmas. Their high LILE/HFSE and LREE/HFSE ratios are interpreted as supra-subduction zone signatures, where LILE-enriched aqueous fluids derived from the down-going slab have modified the depleted mantle wedge, which then melts to generate arc-like basaltic magmas (e.g., Stern, 2002; Tatsumi et al., 1986).

4.2. Crustal sequence of the Gogher–Baft ophiolite

4.2.1. Massive and pillowed lavas

Massive and pillowed lavas are basaltic to basaltic andesitic, with 49.3 to 53 wt.% SiO_2 (Appendix 4). The lavas are fractionated, with Mg# from 36.3 to 53. Pillow lavas are more MORB-like, with higher TiO_2, Zr and Ti/V ratio (Appendix 4) whereas massive lavas are more arc-like, with lower TiO_2, Zr and Ti/V ratio. In Ti vs. V discrimination diagram of Shervais (1982), the pillow lavas have MORB (to slightly OIB-like) characteristics similar to Oman V1 lavas, whereas massive lavas have low Ti/V and display IAT signature (Fig. 8).

Pillow lavas show LREE enrichment (Fig. 7G) with $La_{(N)}/Yb_{(N)}$ between 4.8 and 5.7. Relative to N-MORB, pillow lavas are enriched in HFSE and LILE (Fig. 7H). Pillow lava compositions resemble E-MORB (e.g., enriched in LREE/HREE and HFSE/LREE) albeit showing slight U enrichment or Nb depletion (e.g., Nb/U ~ 0.6 × N-MORB; Nb/U = 46.1 for E-MORB (Sun and McDonough, 1989)). Low Nb/U may reflect

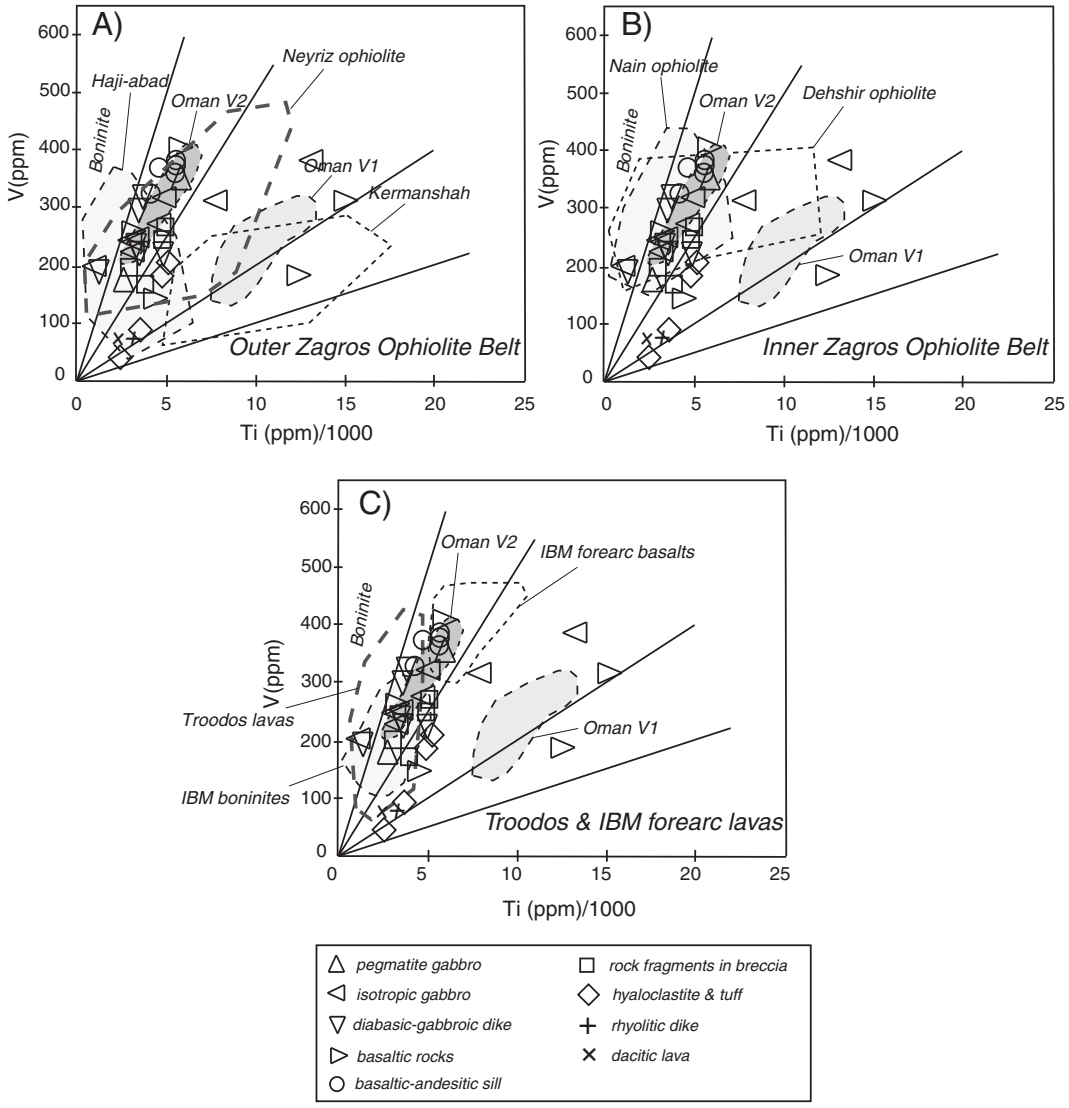

Fig. 8. Plot of the Gogher–Baft lavas on the Ti vs. V diagram (after Shervais, 1982). Most Gogher–Baft rocks occupy IAT (Ti/V > 10) field, although some mafic rocks fall into MORB/BABB and boninite fields. Fields for the V_1 (lower, Geotimes unit) and V_2 (upper, Lasail unit) lavas of the Oman ophiolite are from Alabaster et al. (1982) and Godard et al. (2006). For comparison, fields for outer Zagros ophiolites (A) (including Kermanshah, Neyriz and Haji-Abad ophiolites), inner Zagros ophiolites (B) (Nain and Dehshir ophiolites) and Troodos lavas, with lavas from IBM fore-arc (C) are shown. Nearly all lavas from the inner ophiolitic belt plot in IAT and boninite fields while the Neyriz lavas are distinguished by both fore-arc and boninite-like Ti/V ratios. Some Haji-Abad lavas show MORB characteristics whereas Kermanshah calc-alkaline lavas are represented by high Ti/V, such as Oman V1 lavas. Data for Nain ophiolite is from Shafaii Moghadam (2009), for Dehhsir ophiolite from Shafaii Moghadam et al. (2010); for Haji-Abad from Shafaii Moghadam et al. (2012b) and for Kermanshah and Neyriz ophiolites are unpublished data. Data for Troodos and Izu-Bonin–Marian forearc basalts are from Pearce et al. (1992) and Reagan et al. (2010) respectively.

contribution of slab-derived components to the asthenospheric mantle source during the early stages of subduction. In contrast, massive lava flows exhibit slight LREE depletion (Fig. 7G), Nb–Ti depletion and LILE enrichment on a multi-element N-MORB-normalized diagram (Fig. 7H). The total REE abundance is low in sample BT06-15, similar to boninite, whereas sample BT06-13 shows IAT signature.

4.2.2. Basaltic–andesitic sills in pyroclastic rocks

Basaltic–andesitic sills intruding pyroclastic rocks contain 50.1 to 54.4 wt.% SiO_2 and are fractionated with Mg# = 43.9 to 50 (Appendix 4). These rocks are somewhat altered with relatively high LOI (Appendix 4) and tend to plot in the IAT field on the Ti/V diagram of Shervais (1982), similar to Oman V2 lavas (Fig. 8). Sill samples are characterized by flat REE patterns and seem to be co-genetic, following similar trends (Fig. 7I). The rocks display negative Nb and Ti anomalies (and positive anomalies of LILE relative to LREE (Fig. 7J). Such geochemical characteristics resemble island-arc tholeiitic lavas erupted above subduction zones.

4.2.3. Rock fragments in pyroclastics

Rock fragments in pyroclastics (including pillow fragments in cold breccias) contain 43.9 to 60.8 wt.% SiO_2 (Appendix 4) and are basaltic to andesitic. Most samples plot in the IAT field on the Ti/V diagram of Shervais (1982) (Fig. 8) except for calc-alkalic sample BT06-38. The breccia fragments show fractionated REE patterns with high LREE/HREE ratio (Fig. 7I & J). On a multi-element N-MORB-normalized diagram, breccia fragments have negative HFSE and positive LILE anomalies relative to LREE (Fig. 7J), similar to calc-alkaline lavas.

4.2.4. Pyroclastic units

Pyroclastic units of the Gogher–Baft ophiolite include andesitic hyaloclastites, rhyolitic dikes injected into hyaloclastites, volcanic breccias, tuffs and dacitic lavas as small lenses within breccias. The andesitic hyaloclastites have 58–59 wt.% SiO_2 with relatively low LOI (~2.2 wt.%). These have Ti/V > 24 and plot in MORB field on the Ti/V diagram (Fig. 8). Hyaloclastites have LREE depleted patterns (Fig. 7K) along with depletion in Nb–Ta–Ti and enrichment in LILEs

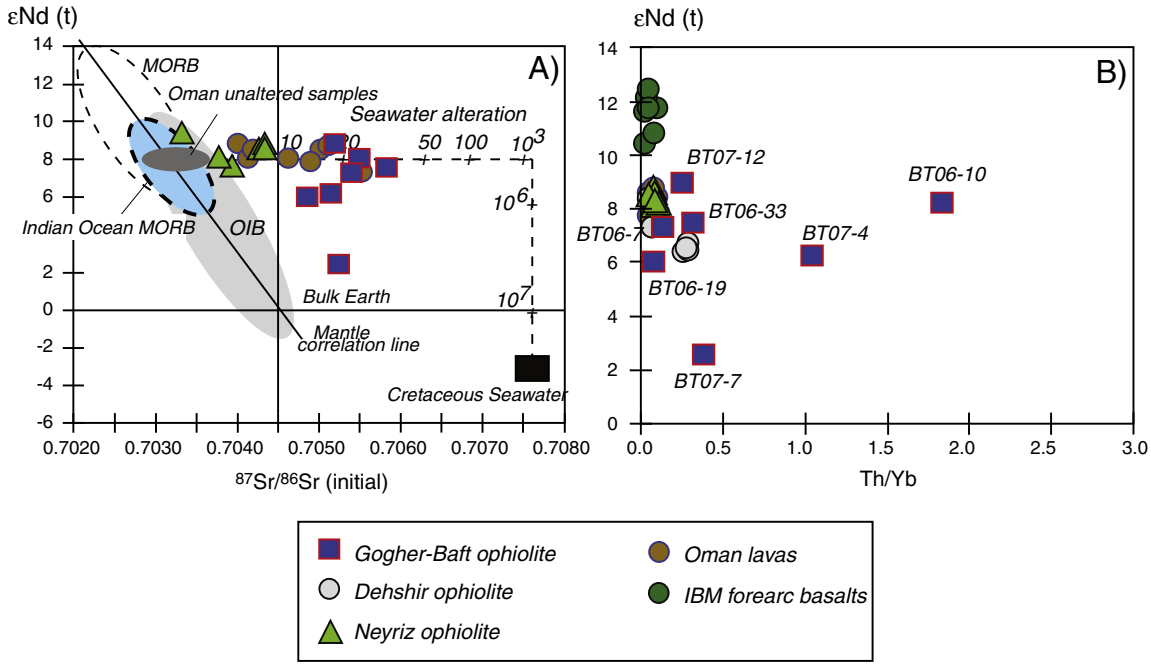

Fig. 9. (A) εNd versus $^{87}Sr/^{86}Sr$ ratios for the Gogher–Baft magmatic rocks, recalculated at 100 Ma. The dashed line indicates the effect of contamination by Cretaceous seawater for different water/rock ratios (modified after Godard et al., 2006). (B) εNd versus Th/Yb for Gogher–Baft magmatic rocks and comparison with lavas from other Late Cretaceous ophiolites and IBM forearc basalts. Data for Oman lavas are from Godard et al. (2006), Neyriz lavas are from Shafaii Moghadam et al., (unpublished data), Dehshir ophiolite from Shafaii Moghadam et al. (2012a) and IBM forearc basalts from Reagan et al. (2010) (colored figure for online version).

relative to LREE in N-MORB-normalized multi-elements diagram (Fig. 7L), similar to island-arc tholeiites.

Tuffs constitute another important member of Gogher–Baft pyroclastic units and show significant alteration (LOI ~ 3–8 wt.%). These are more felsic than underlying ophiolitic units. Tuffs display both LREE-depleted (BT06-1) and enriched (BT06-11) patterns (Fig. 7K). Tuffs also show strong HFSE depletion and LILE enrichment (Fig. 7L), consistent with a calc-alkalic (BT06-11) and island-arc tholeiitic (BT06-1) nature.

The rhyolitic dike is similar to andesitic hyaloclastites, showing LREE-depletion (Fig. 7K), enrichment in LILE and depletion in Nb–Ta (Fig. 7L). The dacitic lava has a highly fractionated REE pattern with $La_{(N)}/Yb_{(N)} \sim 7$ (Fig. 7K). Depletion in HFSE and enrichment in LILE, especially Ba and Th (Fig. 7K) confirm the shoshonitic nature of this sample.

4.3. Sr–Nd–Pb isotope geochemistry

Initial εNd (t) values calculated at 100 Ma (the crystallization age of Inner Belt ophiolites) range from +2.6 to +9 for Gogher–Baft magmatic rocks (Table 1). Rhyolitic dike (BT06-7), andesitic fragment in breccias (BT06-10), isotropic gabbro (BT06-33) and diabasic dike (BT07-12, IAT) are more radiogenic compared to pillow lava (BT07-4), basaltic sill (BT06-19) and calc-alkaline diabasic dike (BT07-7). Samples with more radiogenic Nd overlap with the least radiogenic area of the MORB domain and with Oman and other Late Cretaceous Tethyan ophiolitic rocks (Fig. 9 A). E-MORB type pillow lava and basaltic sill samples have similar εNd (t) values. Sample BT07-12 with higher εNd (t) shows lower REE content compared to other diabasic dikes (Fig. 7E).

Initial $^{87}Sr/^{86}Sr$ calculated at 100 Ma range from 0.7048 to 0.7057 (Table 1), higher than for oceanic tholeiites and likely do not represent the magmatic Sr isotope signature of the rocks. This shift toward higher $^{87}Sr/^{86}Sr$ ratios is commonly attributed to exchange between rock and seawater during alteration (Kawahata et al., 2001; McCulloch et al., 1981), but Sr isotopic determinations of mineral separates such as magmatic clinopyroxene or hornblende is needed to confirm this suspicion.

The initial Pb isotopic ratios range from 38.06 to 38.91 for $^{208}Pb/^{204}Pb$, from 15.50 to 15.64 for $^{207}Pb/^{204}Pb$ and from 17.9 to 18.87 for $^{206}Pb/^{204}Pb$ (Table 1). The magmatic rocks plot above the NHRL in $^{208}Pb/^{204}Pb$ and $^{207}Pb/^{204}Pb$ versus $^{206}Pb/^{204}Pb$ diagram, similar

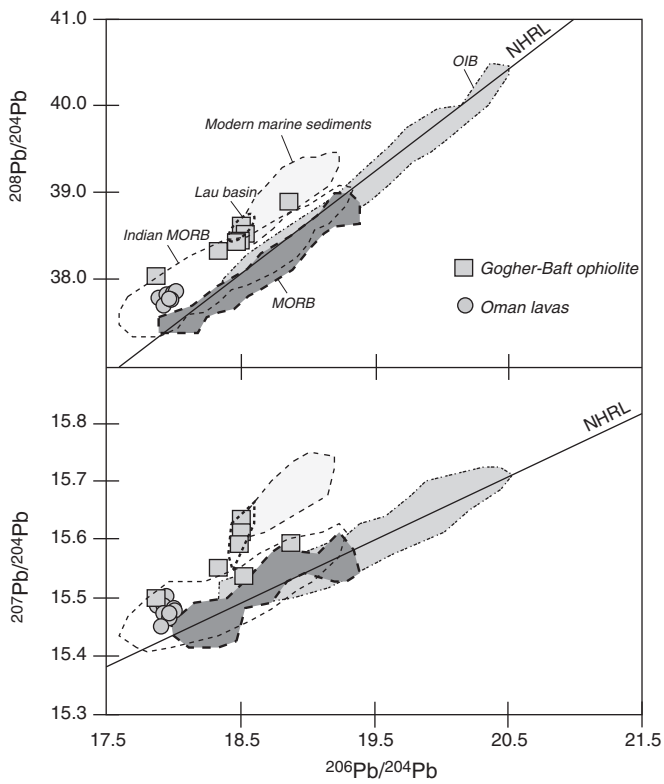

Fig. 10. $^{208}Pb/^{204}Pb$ and $^{207}Pb/^{204}Pb$ against $^{206}Pb/^{204}Pb$ for Gogher–Baft ophiolites recalculated at 100 Ma (modified after Godard et al., 2006). Data for Oman lavas are from Godard et al. (2006).

to Indian Ocean MORB (Fig. 10). Diabasic dikes (BT07-7 and BT07-12) and isotropic gabbro (BT06-33) show high $^{207}Pb/^{204}Pb$ at similar $^{206}Pb/^{204}Pb$ (Fig. 10), which is often interpreted as a crustal and/or slab-derived contribution (Godard et al., 2006). The magmatic rocks plot within least radiogenic area of modern marine sediments and overlap in $^{207}Pb/^{204}Pb$ with Lau Basin lavas (Fig. 10).

Isotopic compositions of Gogher–Baft magmatic rocks reflect different involvement of sediment or crust in their mantle source, either as melt and/or slab-releasing fluids, as implied by variable Th/Yb ratios (Fig. 9B). Samples with radiogenic Nd, show lower Th/Yb except for calc-alkaline sample BT07-7 and sample BT06-10, which both show radiogenic Nd and high Th/Yb. IBM forearc basalts (Reagan et al., 2010), Oman lavas (Godard et al., 2006) and Neyriz ophiolite (Shafaii Moghadam et al., unpublished data) show similar high radiogenic Nd with low Th/Yb. These are mostly MORB-like lavas with a slight signature of subducted components.

5. Discussion

Below we consider three implications of the new data we have presented. First, we address the question of how Gogher–Baft ophiolitic magmas were generated. Then we compare and contrast Gogher–Baft with other Zagros ophiolites. Finally, we use our new results for the Gogher–Baft ophiolite to interpret the tectonic and geodynamic setting in which this ophiolite formed.

5.1. Petrogenesis of Gogher–Baft ophiolites: SSZ vs. MORB setting

Most Gogher–Baft mantle peridotites are harzburgite, with low CaO (<1.0%) and Al_2O_3 (<1.3%) contents similar to modern fore-arc peridotites but overlapping with mid-oceanic ridge peridotites. Gogher–Baft mantle peridotites are similar to South Sandwich forearc peridotites, where harzburgite residues were subsequently modified into slightly enriched peridotites as a result of interaction with arc magmas (Pearce et al., 2000). Harzburgite spinels show medium Cr# (~45 to 53) along with low TiO_2, similar to those from fore-arc harzburgites (Fig. 5). These spinel Cr# are mostly higher than those of typical MOR spinels, and could be residues after moderate degrees of melting. Forearc mantle peridotite is composed of depleted harzburgite, characterized by spinels mostly with Cr#>50 and low TiO_2 contents (Bloomer and Hawkins, 1983; Parkinson and Pearce, 1998; Stern, 2010). Gogher–Baft chromitite probably formed from a boninitic melt. Chromitites with high Cr# spinel are not reported from normal ocean floor, but are common from forearcs (e.g., Arai, 1994, 1997). Gogher–Baft ophiolite magmatic units include diverse magma types: island-arc tholeiitic, calc-alkaline, boninitic as well as E-MORB-type magmas.

The Gogher–Baft ophiolite extrusive sequence consists of older basalt and basaltic andesite pillowed to massive flows (with E-MORB and IAT signatures), changing upward to andesite, dacite and rhyolite (with calc-alkaline, IAT and boninitic affinities). Our new geochemical data suggest that there are four main types of mafic as well as felsic magmas. These are: 1) the early E-MORB pillow lavas and T-MORB gabbros 2) island-arc tholeiites, 3) calc-alkaline rocks, and 4) late stage boninitic lavas. The late-stage magmas, like those injected into the pyroclastic rocks, also display IAT signature. Dacitic lava in pyroclastic rocks possesses a shoshonitic character. The negative Nb–Ta and positive LILE anomalies (relative to LREE on N-MORB normalized multi-element diagrams) obtained from these magmatic rocks clearly indicate a supra-subduction zone tectonic environment (Fig. 7). In chondrite-normalized REE diagrams, flat to slightly LREE depleted patterns and very low REE concentrations are characteristic of IAT and boninitic series respectively. These characteristics are commonly found in the supra-subduction zone-type ophiolites of the Eastern Mediterranean region (e.g., Al-Riyami et al., 2002; Bagci and Parlak, 2009; Parlak et al., 2000; Yaliniz et al., 1996) as well as in other Zagros Late Cretaceous ophiolites (Shafaii Moghadam and Stern, 2011). The presence of boninitic rocks has been documented in southern Mediterranean ophiolites including Kizildag (Hatay) (Bagcý et al., 2008), Tekirova (Antalya) (Bagci and Parlak, 2009), Baer-Bassit in northern Syria (Al-Riyami et al., 2002), Troodos in Cyprus (Dilek and Flower, 2003) as well as from Oman ophiolites. Boninitic magmatism is also common in other Late Cretaceous Zagros ophiolites (Shafaii Moghadam and Stern, 2011).

E-MORB-type pillow lavas are similar to Late Cretaceous OIB-type dikes intruding Tauride belt ophiolites of Turkey (Celik and Delaloye, 2003; Parlak et al., 2006), and have also been reported from the Haji-Abad ophiolite (Outer Belt) (Shafaii Moghadam and Stern, 2011). εNd of Gogher–Baft E-MORB lavas are similar to least radiogenic MORB domain and/or to OIB lavas (Fig. 9A), but show slightly more radiogenic Pb, similar to Indian MORBs (Fig. 10). The occurrence of E-MORB in these ophiolites has been suggested to be the result of late-stage off-axis magmatism fed by melts that possibly originated within an asthenospheric window due to slab break-off, shortly after the emplacement of the ophiolites (Shervais, 2001). These E-MORB-type igneous rocks could also be interpreted as the first magmas generated when the Tethyan oceanic plate began to subduct beneath Eurasia in the Late Cretaceous. We infer that these melts were generated from a mantle source that was not yet depleted or affected by subduction components, perhaps flowing in from beneath Eurasia to fill the space created by the initial sinking of the Tethyan plate as hypothesized by Stern and Bloomer (1992).

The Th/Yb vs. Ta/Yb diagram (Fig. 11) discriminates between depleted mantle (MORB) and enriched mantle (OIB) sources (Pearce et al., 1995). For subduction-related magmatic rocks, the addition of elements such as Th, by slab-derived fluids/melts increases the Th/Yb in the mantle source as shown by the arrow in Fig. 11. Nearly all the samples from the present study show strong SSZ signature, with higher Th/Yb ratio, except the pillow lavas and pegmatite gabbros with E-MORB/OIB and E-MORB characteristics (Fig. 11).

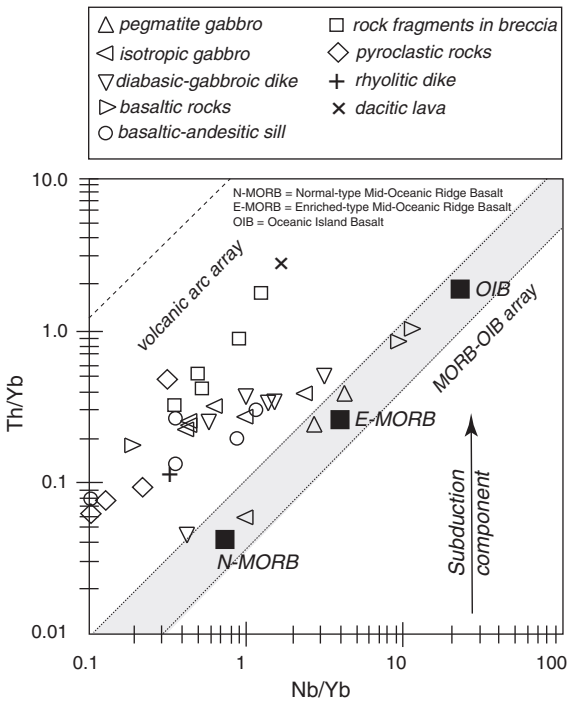

Fig. 11. Th/Yb vs. Nb/Yb diagram (after Leat et al., 2004) for the Gogher–Baft ophiolite. Most magmatic units from the Gogher–Baft ophiolite have high Th/Yb and plot above the mantle array near the volcanic arc array, with some exceptions that are E-MORB to N-MORB-like.

5.2. Comparison with other Late Cretaceous Zagros ophiolites

Here we briefly compare geochemical features of both Outer Belt (Kermanshah, Neyriz and Haji-Abad) and Inner Belt Ophiolites (Nain, Dehshir, Shahr-e-Babak and Gogher–Baft) to better reconstruct the geochemical evolution and hence to evaluate their geodynamic setting.

As spinel composition is widely accepted to reflect the geodynamic setting of host peridotites, we compare these from both inner and outer ophiolite belts. Nearly all spinels from inner and outer belt ophiolites as well as Semail ophiolitic peridotites are similar to those of forearc harzburgites with some similar to abyssal peridotites (Fig. 5).

Geochemical signatures of Gogher–Baft magmatic rocks resemble those of both inner and outer belt Zagros ophiolitic lavas. Most inner and outer belt ophiolite lavas fall within the IAT and boninitic fields on Ti/V diagram of Shervais (1982), and are similar to both depleted Lasail (V2) lavas of Oman and to Troodos lavas (Fig. 8). These lavas are also similar to fore-arc basalts (Ishizuka et al., 2011; Reagan et al., 2010) and to boninites from the Izu-Bonin–Mariana fore-arc (Fig. 8). Some samples from Zagros inner and outer belt ophiolites (like as MORB-like Haji-Abad lavas) are MORB-like, similar to V1 lavas of the Semail ophiolite. Neyriz ophiolite lavas are compositionally intermediate between tholeiitic lavas of the Oman Geotimes unit and depleted lavas of the Lasail unit, similar to Izu-Bonin–Mariana fore-arc basalts (Fig. 8). Available εNd (t) for Late Cretaceous Neotethyan ophiolites including Troodos, Oman, Dehshir, Neyriz and Gogher–Baft ophiolites are shown in Fig. 12. Most Troodos boninitic upper lavas and one Gogher–Baft ophiolite lava with calc-alkaline signatures have less radiogenic Nd than Oman, Neyriz and Dehshir ophiolitic lavas. The mantle source of samples with less radiogenic Nd may have been strongly affected by subducted sedimentary components.

5.3. Tectonic setting and geodynamic evolution of Gogher–Baft ophiolites

Magmatic rocks in ophiolites provide valuable information about crustal accretion processes in different tectono-magmatic environments. Volcanic sequences in an ophiolite sometimes display varying geochemical characteristics, indicating spatial and/or temporal modification of mantle sources as this evolved (e.g., Pearce et al., 1984). Many ophiolites are thus recognized to have formed in a supra-subduction zone (SSZ) environment (e.g., Miyashiro, 1974; Pearce et al., 1984; Shervais, 2001 and references therein; Dilek et al., 2007; Yellappa et al., 2011), including island arc, fore-arc and back-arc basins where new oceanic lithosphere is generated. SSZ-type ophiolites usually contain a geochemical stratigraphy which includes IAT, boninites, and calc-alkaline magmatic rocks with minor MORB-like lavas (Pearce, 2003; Pearce et al., 1984). The "Subduction Initiation Rule" provides important guidelines for ophiolites that formed in a forearc during subduction initiation (SI; Whattam and Stern, 2011), specifically that early SI magmas are MORB-like and become increasingly arc-like with time.

Neo-Tethyan ophiolites on the southern flank of Eurasia formed in a SSZ setting, about the same time ~90–100 Ma. (Shafaii Moghadam et al., 2013) The southern branch of Neo-Tethys comprises well-documented ophiolites such as the Tekirova (Antalya), Kizildag (Hatay), Ispendere (Malatya) in Turkey (Bagci and Parlak, 2009; Bagcý et al., 2005; Parlak and Robertson, 2004), Troodos in Cyprus (Dilek and Flower, 2003), Baer Bassit in Syria (Al-Riyami et al.,

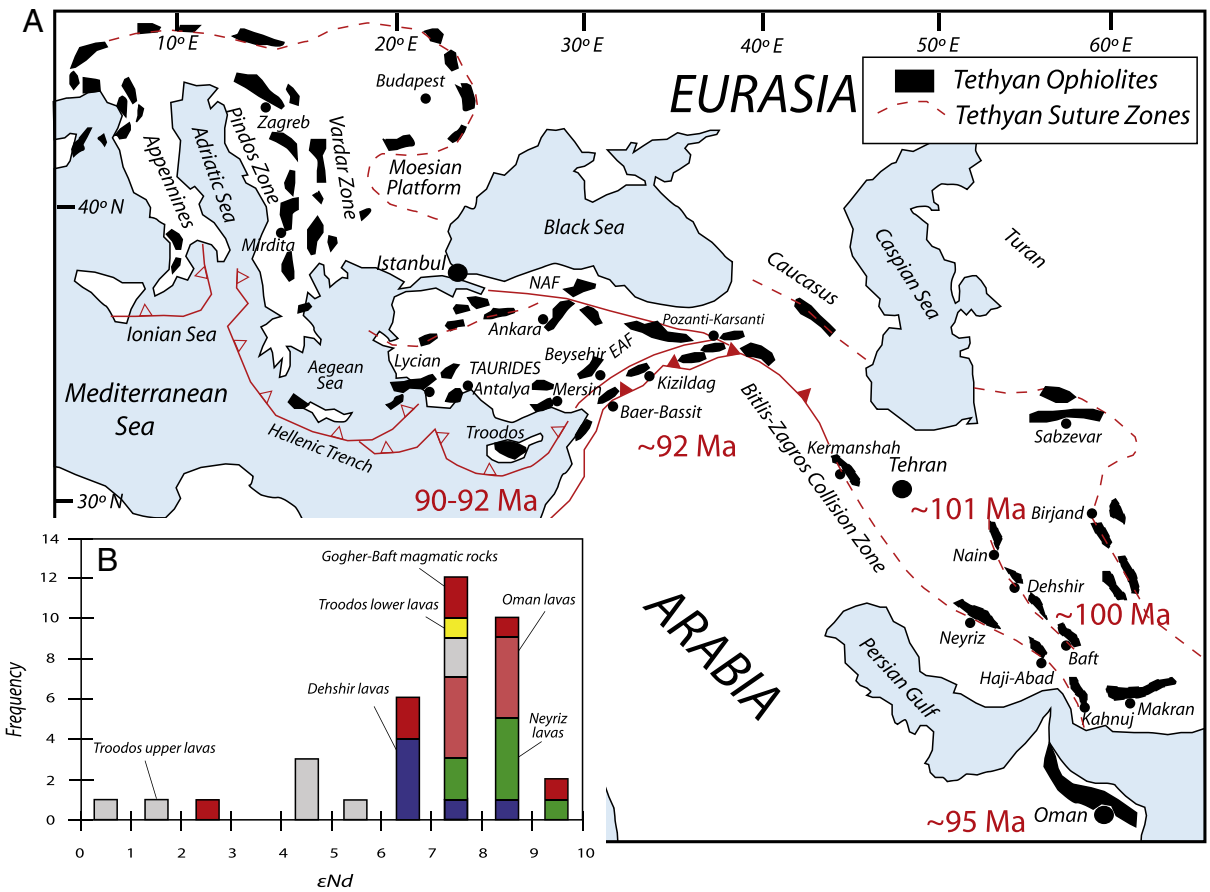

Fig. 12. (A) Simplified tectonic map of the eastern Mediterranean-Zagros region showing the distribution of the Neotethyan ophiolites and suture zones (modified after Dilek et al., 2007). (B) Histograms compares avaiable εNd (t) data for Troodos, Oman, Dehshir, Neyriz and Gogher–Baft ophiolites. Data are from Godard et al. (2006), McCulloch and Cameron (1983) and Shafaii Moghadam et al., (unpublished data) for Oman, Troodos and Neyriz respectively (colored figure for online version).

2002) and Zagros ophiolites (including Gogher–Baft) in Iran (Shafaii Moghadam and Stern, 2011).

The first lavas in Tethyan ophiolites (including Zagros late Cretaceous ophiolites) as well as Izu-Bonin–Mariana fore-arc basalts tend to be MORB-like (and/or IAT), whereas younger ophiolitic lavas display IAT, boninitic and calc-alkalic characteristics. Boninites are found in many other ophiolitic complexes (Bédard et al., 1998; among others). Modern boninites are mainly restricted to fore-arc environments such as those of the Izu-Bonin–Mariana fore-arc (e.g., Stern, 2004; Stern and Bloomer, 1992), although boninites are also common in the N. Lau Basin, near its termination with a plate-bounding transform to the north (Falloon et al., 2007). The present position of Zagros Late Cretaceous ophiolites in a forearc along with the presence of IAT, calc-alkalic and boninitic lavas suggest that they formed in a fore-arc over a rapidly evolving supra-subduction zone setting in the southern Neo-Tethys (Shafaii Moghadam and Stern, 2011). In this scenario, a broad and continuous tract of oceanic lithosphere formed at about the same time during Late Cretaceous time along the southern margin of Eurasia. According to this model, the Zagros Outer and Inner Belt ophiolites are remnants of a once-continuous tract of fore-arc lithosphere that was created about the same time in association with a new subduction zone. This fore-arc tract extended beyond Iran through Syria and Turkey as far as Cyprus to the west and Oman to the east. Such a fore-arc model is increasingly proposed for eastern Mediterranean Late Cretaceous ophiolites (e.g., Bagcý et al., 2005, 2006, 2008; Dilek and Thy, 2009; Dilek et al., 2007; Parlak et al., 2009).

All Zagros ophiolites (both Outer and Inner Belt) are dominated by components with strong supra-subduction zone affinity, from mantle harzburgites to overlying magmatic rocks with some MORB-like lava. MORB-like lavas are usually older than the arc-like lavas. These lithological and geochemical variations in ophiolites are traditionally explained by a shift in tectonic setting from mid-oceanic ridge to island-arc and/or two distant mantle sources for generating magmatic rocks (e.g., Portnyagin et al., 1997). More recently, this compositional bimodality has been ascribed to progressive depletion and subduction-related metasomatism of the mantle source during ophiolite formation. According to this model, all ophiolite magmatic rocks (MORB, IAT, boninites) formed in the same fore-arc region, beginning with eruption of early MORB-like tholeiites (fore-arc basalts "FAB" of Reagan et al., 2010) and evolving to younger boninitic lavas (Whattam and Stern, 2011). This is consistent with the observation in the Izu-Bonin–Mariana forearc that earlier MORB-like basaltic lavas (FAB) were followed by boninitic magmatism (Ishizuka et al., 2011; Reagan et al., 2010). The fore-arc/subduction initiation scenario for the Zagros ophiolites is mostly consistent with the occurrence of boninites and depleted harzburgites with high Cr# number ($40<Cr\#<80\%$) in these ophiolites. The forearc ophiolites have similar ages, varying from 90–94 Ma for Cyprus (Mukasa and Ludden, 1987), ~95 Ma and/or 99–100 Ma for Oman ophiolites (Goodenough et al., 2010; Tsuchiya et al., 2013; Warren et al., 2005), 92–93 Ma for Neyriz (Outer Belt) (Babaie et al., 2006) and 101–103 Ma for Nain-Dehshir (Inner Belt) ophiolites (Shafaii Moghadam et al., 2013), consistent with a model whereby subduction initiation began along the Iran margin and propagated E and W with time.

6. Conclusions

The Late Cretaceous Gogher–Baft ophiolite is a slice of the Neo-Tethyan oceanic lithosphere within the Inner Zagros Ophiolitic Belt.

Depleted mantle harzburgites, pegmatite and isotropic gabbros, pillow lavas and andesitic–dacitic massive lavas with overlying pyroclastic rocks are the main rock units. Layered ultramafic–mafic cumulates, crustal isotropic gabbros, and sheeted dike complex are not recognized. Turonian to Maastrichtian pelagic sediments cover and/or are interbedded with both ophiolitic lavas and pyroclastic rocks.

Mantle harzburgites have depleted geochemical signatures, characterized by moderate to high Cr# similar to those from fore-arc and abyssal harzburgites. Chromitites probably formed from a boninitic melt.

Gogher–Baft magmatic rocks have supra-subduction zone affinity, but rare MORB-type lavas also exist. Sr isotopic compositions may reflect the effects of seawater alteration. Nd isotope compositions of Gogher–Baft magmatic rocks reflect variable involvement of sediment components in the mantle source, introduced as either melt or fluids. Lead isotopic compositions plot systematically above the NHRL, overlapping with least radiogenic marine sediments and Lau Basin lavas.

Zagros outer and inner belt ophiolites and other Late Cretaceous Neo-Tethyan ophiolites along the Bitlis-Zagros suture zone, show many similarities including the age of overlying sediments, age of magmatism, lithological variations and geochemical evolution. The similarity of ages for magmatic rocks and overlying sediments suggests that Zagros inner and outer ophiolite belts are the exposed limbs of a single deformed sheet, which formed as a magmatic forearc to the Cretaceous and younger igneous rocks of the Urumieh–Dokthar arc and also acted as backstop to the growing Zagros accretionary prism. In this scenario, the Zagros ophiolites formed when northeast-directed subduction began beneath southern Eurasia, from Cyprus to Oman, beginning about 100 Ma and thus record a complex history of supra-subduction zone formation adjacent to Eurasia.

Supplementary data to this article can be found online at http://dx.doi.org/10.1016/j.lithos.2013.01.013.

Acknowledgments

We are very grateful to Tomoaki Morishita and Ibrahim Uysal for their constructive reviews of the manuscript. Editorial suggestions by Dr. Andrew Kerr are highly appreciated.

References

Agard, P., Monie, P., Gerber, W., Omrani, J., Molinaro, M., Meyer, B., Labrousse, L., Vrielynck, B., Jolivet, L., Yamato, P., 2006. Transient, synobduction exhumation of Zagros blueschists inferred from P–T, deformation, time, and kinematic constraints: implications for Neo-Tethyan wedge dynamics. Journal of Geophysical Research 111, B11401. http://dx.doi.org/10.1029/2005JB004103.

Alabaster, T., Pearce, J.A., Malpas, J., 1982. The volcanic stratigraphy and petrogenesis of the Oman ophiolite. Contributions to Mineralogy and Petrology 81, 168–183.

Al-Riyami, K., Robertson, A., Dixon, J., Xenophontos, C., 2002. Origin and emplacement of the Late Cretaceous Baer–Bassit ophiolite and its metamorphic sole in NW Syria. Lithos 65, 225–260.

Arai, S., 1994. Characterization of spinel peridotites by olivine-spinel compositional relationships: review and interpretation. Chemical Geology 113, 191–204.

Arai, S., 1997. Origin of podiform chromitites. Journal of Asian Earth Sciences 15, 303–310.

Arvin, M., Robinson, P.T., 1994. The petrogenesis and tectonic setting of lavas from the Baft ophiolitic mélange, southwest of Kerman, Iran. Canadian Journal of Earth Sciences 31, 824–834.

Arvin, M., Shokri, E., 1996. Genesis and eruptive environment of basalts from the Gogher ophiolitic mélange, southwest of Kerman, Iran. Ofioliti 22, 175–182.

Babaie, H.A., Ghazi, A.M., Babaei, A., La Tour, T.E., Hassanipak, A.A., 2001. Geochemistry of arc volcanic rocks of the Zagros Crush Zone, Neyriz, Iran. Journal of Asian Earth Sciences 19, 61–76.

Babaie, H.A., Babaei, A., Ghazi, A.M., Arvin, M., 2006. Geochemical, $^{40}Ar/^{39}Ar$ age, and isotopic data for crustal rocks of the Neyriz ophiolite, Iran. Canadian Journal of Earth Sciences 43, 57–70.

Bagci, U., Parlak, O., 2009. Petrology of the Tekirova (Antalya) ophiolite (Southern Turkey): evidence for diverse magma generations and their tectonic implications during Neotethyan-subduction. International Journal of Earth Sciences 98, 387–405.

Bagcý, U., Parlak, O., Hock, V., 2005. Whole rock and mineral chemistry of cumulates from the Kýzýldag (Hatay) ophiolite (Turkey): clues for multiple magma generation during crustal accretion in the southern Neotethyan Ocean. Mineralogical Magazine 69, 53–76.

Bagcý, U., Parlak, O., Hock, V., 2006. Geochemical character and tectonic environment of ultramafic to mafic cumulates from the Tekirova (Antalya) ophiolite (Southern Turkey). Geological Journal 41, 193–219.

Bagcý, U., Parlak, O., Hock, V., 2008. Geochemistry and tectonic environment of diverse magma generations forming the crustal units of the Kizildag (Hatay) ophiolite southern Turkey. Turkish Journal of Earth Sciences 17, 43–71.

Bédard, J.H., Lauzière, K., Tremblay, A., Sangster, A., 1998. Evidence from Betts Cove ophiolite boninites for forearc seafloor-spreading. Tectonophysics 284, 233–245. http://dx.doi.org/10.1016/S0040-1951(97)00182-0.

Berberian, M., King, G.C.P., 1981. Towards a paleogeography and tectonic evolution of Iran. Canadian Journal of Earth Sciences 18, 210–265.

Bloomer, S.H., Hawkins, J.W., 1983. Gabbroic and ultramafic rocks from the Mariana Trench: an island arc ophiolite. In: Hayes, D.E. (Ed.), The Tectonic and Geologic Evolution of Southeast Asian Seas and Islands Part 2: American Geophysical Union, Geophysical Monograph, 27, pp. 94–317.

Bodinier, J.L., Vasseur, G., Vemieres, J., Dupuy, C., Fabries, J., 1990. Mechanisms of mantle metasomatism: geochemical evidence from the Lherz orogenic peridotite. Journal of Petrology 31, 597–628.

Braud, J., 1970. Les formations du Zagros dans la region de Kermanshah (Iran) et leurs rapports structuraux. Comptes Rendus de l'Académie des Sciences 271, 1241–1244.

Braud, J., 1978. Geological map of Kermanshah 1/250000 scale. Geological Survey of Iran.

Celik, O.F., Delaloye, M., 2003. Origin of metamorphic soles and their post-kinematic mafic dyke swarms in the Antalya and Lycian ophiolites, SW Turkey. Geological Journal 38, 235–256.

Davoudzadeh, M., 1972. Geology and Petrography of the Area North of Nain, Central Iran. Geological Survey of Iran, report No.14.

De Bari, S.M., Coleman, R.G., 1989. Examination of the deep levels of an island-arc: evidence from the Tunisia ultramafic–mafic assemblage, Tonisia, Alaska. Journal of Geophysical Research 94, 4373–4391. http://dx.doi.org/10.1029/JB094iB04p04373.

Delaloye, M., Desmons, J., 1980. Ophiolites and mélange terranes in Iran: a geochronological study and its paleotectonic implications. Tectonophysics 68, 83–111.

Desmons, J., Beccaluva, L., 1983. Mid-ocean ridge and island arc affinities in ophiolites from Iran: palaeographic implications. Chemical Geology 39, 39–63.

Dick, H.J.B., Bullen, T., 1984. Chromian spinel as a petrogenetic indicator in abyssal and Alpine-type peridotites and spatially associated lavas. Contributions to Mineralogy and Petrology 86, 54–76.

Dilek, Y., Flower, M.F.J., 2003. Arc-trench Rollback and Forearc Accretion: A Model Template for Ophiolites in Albania, Cyprus, and Oman. In: Dilek, Y., Robinson, P.T. (Eds.), Ophiolites in Earth History: Geological Society of London Special Publication, 218, pp. 43–68.

Dilek, Y., Furnes, H., 2009. Structure and geochemistry of Tethyan ophiolites and their petrogenesis in subduction rollback systems. Lithos 113, 1–20.

Dilek, Y., Furnes, H., 2011. Ophiolite genesis and global tectonics: tectonic fingerprinting of ancient oceanic lithosphere. Geological Society of America Bulletin 123, 387–411.

Dilek, Y., Thy, P., 2009. Island arc tholeiite to boninitic melt evolution of the Cretaceous Kizildag (Turkey) ophiolite: model for multi-stage early arc-forearc magmatism in Tethyan subduction factories. Lithos 113, 68–87.

Dilek, Y., Furnes, H., Shallo, M., 2007. Suprasubduction zone ophiolite formation along the periphery of Mesozoic Gondwana. Gondwana Research 11, 453–475.

Dimitrijevic, M.D., 1973. Geology of Kerman. Geological Survey of Iran, No. 72.

Falloon, T.J., Danyushevsky, L.V., Crawford, T.J., Maas, R., Woodhead, J.D., Eggins, S.M., Bloomer, S.H., Zlobin, S.K., Stacey, A.R., 2007. Multiple mantle plume components involved in the petrogenesis of subduction-related lavas from the northern termination of the Tonga Arc and northern Lau Basin: Evidence from the geochemistry of arc and backarc submarine volcanics. Geochemistry, Geophysics, Geosystems 8 (9). http://dx.doi.org/10.1029/2007GC001619.

Floyd, P.A., Yaliniz, M.K., Goncuoglu, M.C., 1998. Geochemistry and petrogenesis of intrusive and extrusive ophiolitic plagiogranites, Central Anatolian Crystalline Complex, Turkey. Lithos 42, 225–241.

Garfunkel, Z., 2006. Neotethyan ophiolites: formation and obduction within the life cycle of the host basins. Geological Society of London, Special Publication 260, 301–326.

Ghazi, A.M., Hassanipak, A.A., 2000. Petrology and geochemistry of the Shahr-Babak ophiolite, Central Iran. Geological Society of America Bulletin, Special Paper 349, 485–497.

Ghazi, A.M., Pessagno, E.A., Hassanipak, A.A., Kariminia, S.M., Duncan, R.A., Babaie, H.A., 2003. Biostratigraphic zonation and ^{40}Ar–^{39}Ar ages for the Neotethyan Knoy ophiolite of NW Iran. Palaeogeography, Palaeoclimatology, Palaeoecology 193, 311–323.

Godard, M., Dautria, J.M., Perrin, M., 2003. Geochemical variability of the Oman ophiolite lavas: relationship with spatial distribution and paleomagnetic directions. Geochemistry, Geophysics, Geosystems 4 (6), 8609. http://dx.doi.org/10.1029/2002GC000452.

Godard, M., Bosch, D., Einaudi, F., 2006. A MORB source for low-Ti magmatism in the Semail ophiolite. Chemical Geology 234, 58–78.

Goodenough, K.M., Style, M.T., Schofield, D., Thomas, R.J., Crowley, Q.C., Lilly, R.M., McKervey, J., Stephenson, D., Carney, J.N., 2010. Architecture of the Oman-UAE ophiolite: evidence for a multi-phase magmatic history. Arabian Journal of Geosciences 3, 439–458.

Gruau, G., Griffi ths, J.B., Lecuyer, C., 1998. The origin of U-shaped rare earth patterns in ophiolite peridotites: assessing the role of secondary alteration and melt/rock reaction. Geochimica et Cosmochimica Acta 62, 3545–3560. http://dx.doi.org/10.1016/S0016-7037(98)00250-6.

Hawkins, J.W., Allan, J.F., 1994. Petrologic evolution of Lau Basin sites 834 through 839. In: Hawkins, J.W., et al. (Ed.), Proceedings of the Ocean Drilling Program, Scientific Results: Volume 135: College Station, Texas, Ocean Drilling Program, pp. 427–470.

Hébert, R., Adamson, A.C., Komor, S.C., 1990. Metamorphic petrology of ODP 109, Hole 670A serpentinized peridotites: serpentinization processes at a slow spreading ridge environment. In: Detrick, R., Honnorez, J., Bryan, W.B., et al. (Eds.), Proceedings of the Ocean Drilling Program, Scientific Results 106/109, College Station, Texas, pp. 103–115.

Hout, F., Hebert, R., Varfalvy, V., Beaudoin, G., Wang, C.S., Liu, Z.F., Cotten, J., Dostal, J., 2002. The Beimarang melange (southern Tibet) brings additional constraints in assessing the origin, metamorphic evolution and obduction processes of the Yarlung Zangbo ophiolite. Journal of Asian Earth Sciences 21, 307–322.

Ishii, T., Robinson, P.T., Maekawa, H., Fiske, R., 1992. Petrological Studies of Peridotites From Diapiric Serpentinite Seamounts in the Izu-Ogazawara-Mariana Forearc, Leg 125. In: Fryer, P., Pearce, J.A., Stokking, L.B., et al. (Eds.), Proceedings of the Ocean Drilling Program, Scientific Results 125, College Station, Texas, pp. 445–485.

Ishizuka, O., Tani, K., Reagan, M.K., Kanayama, K., Umino, S., Harigane, Y., Sakamoto, I., Miyajima, Y., Yuasa, M., Dunkley, D.J., 2011. The timescales of subduction initiation and subsequent evolution of an oceanic island arc. Earth and Planetary Science Letters 306, 229–240.

Johnson, K.T.M., Dick, H.J.B., Shimizu, N., 1990. Melting in the oceanic upper mantle: an ion microprobe study of diopsides in abyssal peridotites. Journal of Geophysical Research 95, 2661–2678.

Kawahata, H., Nohara, M., Ishizuka, H., Hasebe, S., Chiba, H., 2001. Sr isotope geochemistry and hydrothermal alteration of the Oman ophiolite. Journal of Geophysical Research 106, 11083–11099.

Kusky, T.M., 2004. Precambrian ophiolites and related rocks, Developments in Precambrian Geology, 13. Elsevier publications.

Le Mée, L., Girardeau, J., Monnier, C., 2004. Mantle segmentation along the Oman ophiolite fossil mid-ocean ridge. Nature 432, 167–172.

Leat, P.T., Pearce, J.A., Barker, P.F., Millar, I.L., Barry, T.L., Larter, R.D., 2004. Magma genesis and mantle flow at a subducting slab edge: the South Sandwich arc-basin system. Earth and Planetary Science Letters 227, 17–35.

Leterrier, J., Maury, R.C., Thonon, P., Girard, D., Marchal, M., 1982. Clinopyroxene composition as a method of identification of the magmatic affinities of paleo-volcanic series. Earth and Planetary Science Letters 59, 139–154.

McCall, G.J.H., Kidd, R.G.W., 1981. The Makran, Southeastern Iran: The Anatomy of a Convergent Plate Margin Active from Cretaceous to Present. In: Leggett, L. (Ed.), Trench–Fore Arc Geology: Geological Society of London Special Publication, 10, pp. 387–397.

McCulloch, M.T., Gregory, R.T., Wasserburg, G.T., Taylor, H.P., 1981. Sm–Nd, Rb–Sr, and $^{18}O/^{16}O$ isotopic systematics in an oceanic crustal section: evidence from the Samail ophiolite. Journal of Geophysical Research 86, 2721–2735.

McCulloch, M.T., Cameron, W.E., 1983. Nd-Sr isotopic study of primitive lavas from the Troodos ophiolite, Cyprus: evidence for a subduction-related setting. Geology 11, 727–731.

McDonough, W.F., Sun, S.S., 1995. The composition of the Earth. Chemical Geology 120, 223–253.

McQuarrie, N., Stock, J.M., Verdel, C., Wernicke, B.P., 2003. Cenozoic evolution of Neotethys and implications for the causes of plate motions. Geophysical Research Letters 30. http://dx.doi.org/10.1029/2003GL017992.

Mijalkovic, N., Cvetic, S., Dimitrijevic, M. D., 1972. The Geological map of Balvard. 1/100000 Series, Sheet 7248.

Miyashiro, A., 1974. Volcanic rock series in island arcs and active continental margins. American Journal of Science 274, 321–355.

Mukasa, S., Ludden, J.N., 1987. Uranium-lead isotopic ages of plagiogranites from the Troodos Ophiolite, Cyprus, and their tectonic significance. Geology 15, 825–828.

Nelson, S.T., Montana, A., 1992. Sieve-textured plagioclase in volcanic rocks produced by rapid decompression. American Mineralogist 77, 1242–1249.

Niu, Y., 2004. Bulk-rock major and trace element compositions of abyssal peridotites: implications for mantle melting, melt extraction and post-melting processes beneath midocean ridges. Journal of Petrology 1–36.

Parkinson, I.J., Pearce, J.A., 1998. Peridotites from the Izu-Bonin–Mariana forearc (ODP Leg 125): evidence for mantle melting and melt–mantle interaction in a suprasubduction zone setting. Journal of Petrology 39, 1577–1618.

Parlak, O., Robertson, A.H.F., 2004. The ophiolite-related Mersin mélange, southern Turkey: its role in the tectonic-sedimentary setting of the Tethys in the eastern Mediterranean region. Geological Magazine 141, 257–286.

Parlak, O., Hock, V., Delaloye, M., 2000. Suprasubduction zone origin of the Pozanti-Karsanti ophiolite (southern Turkey) deduced from whole-rock and mineral chemistry of the gabbroic cumulates. In: Bozkurt, E., Winchester, J.A., Piper, J.D.A. (Eds.), Tectonics and Magmatism in Turkey and the Surrounding Area: Geological Society of London Special Publication, 173, pp. 219–234.

Parlak, O., Yýlmaz, H., Boztug, D., 2006. Geochemistry and tectonic setting of the metamorphic sole rocks and isolated dykes from the Divrigci ophiolite (Sivas, Turkey): evidence for melt generation within an asthenospheric window prior to ophiolite emplacement. Turkish Journal of Earth Sciences 15, 25–45.

Parlak, O., Rizaoglu, T., Bagci, U., Karaoglan, F., Hock, V., 2009. Tectonic significance of the geochemistry and petrology of ophiolites in southeast Anatolia, Turkey. Tectonophysics 473, 173–187.

Pearce, J.A., 2003. Supra-subduction Zone Ophiolites: The Search for Modern Analogues. In: Dilek, Y., Newcomb, S. (Eds.), Ophiolite: concept and the evolution of geological thought: Geological Society of America Special Paper, 373, pp. 269–293.

Pearce, J.A., Norry, M.J., 1979. Petrogenetic implications of Ti, Zr, Y and Nb variations in volcanic rocks. Contributions to Mineralogy and Petrology 69, 33–47.

Pearce, J.A., Robinson, P.T., 2010. The Troodos ophiolite complex probably formed in a subduction initiation, slab edge setting. Gondwana Research 18, 60–81.

Pearce, J.A., Lippard, L.S., Roberts, S., 1984. Characteristics and tectonic significance of supra-subduction zone ophiolites. Geological Society of London, Special Publication 16, 77–94.

Pearce, J.A., Vander Laan, S.R., Arculus, R.J., Murton, B.J., Ishii, T., Peate, D.W., Parkinson, I.J., 1992. Boninite and harzburgite from Leg 125 (Bonin-Mariana forearc): a case study of magma genesis during the initial stages of subduction. In: Fryer, P., et al. (Ed.), Proceeding of the Ocean Drilling Program, scientific results, Site 778–786. Bonin-Mariana Region, College Station, Texas, pp. 623–659.

Pearce, J.A., Baker, P.E., Harvey, P.K., Luff, I.W., 1995. Geochemical evidence for subduction fluxes, mantle melting and fractional crystallization beneath the South Sandwich arc. Journal of Petrology 36, 1073–1109.

Pearce, J.A., Barker, P.F., Edwards, S.J., Parkinson, I.J., Leat, P.T., 2000. Geochemistry and tectonic significance of peridotites from the South Sandwich arc-basin system, South Atlantic. Contributions to Mineralogy and Petrology 139, 36–53.
Portnyagin, M.V., Danyushevsky, L.V., Kamenetsky, V.S., 1997. Coexistence of two distinct mantle sources during formation of ophiolites: a case study of primitive pillow-lavas from the lowest part of the volcanic section of the Troodos Ophiolite, Cyprus. Contributions to Mineralogy and Petrology 128, 287–301.
Prinzhofer, A., Allègre, C.J., 1985. Residual peridotites and the mechanisms of partial melting. Earth and Planetary Science Letters 74, 251–265. http://dx.doi.org/10.1016/0012-821X(85)90025-1.
Reagan, M.K., Ishizuka, O., Stern, R.J., Kelley, K.A., Ohara, Y., Blichert-Toft, J., Bloomer, S.H., Cash, J., Fryer, P., Hanan, B.B., Hickey-Vargas, R., Ishii, T., Kimura, J.I., Peate, D.W., Rowe, M.C., Woods, M., 2010. Fore-arc basalts and subduction initiation in the Izu-Bonin–Mariana system. Geochemistry, Geophysics, Geosystems 11, Q03X12. http://dx.doi.org/10.1029/2009GC002871.
Ricou, L.E., 1971. Le croissant ophiolitique peri-Arabe une ceinture de nappes mise en place au Cretace superieur. Review Geographie Physique Geologie Dynamique 13, 327–350.
Ricou, L.E., 1976. Evolution structurale des Zagrides. La région clef de Neyriz (Zagros Iranien). Memoire Societé Geologie de la France 125 (140 pp., (Thèse Orsay, 1974)).
Ricou, L.E., Braud, J., Brunn, J.H., 1977. Le Zagros. Memoire Societé Geologie de la France 8, 33–52.
Robertson, A.H.F., 1998. Mesozoic–Tertiary Tectonic Evolution of the Easternmost Mediterranean Area: Integration of Marine and Land Evidence. In: Robertson, A.H.F., Emeis, K.C., Richetr, C., Camerlenghi, A. (Eds.), Proceeding of the Ocean Drilling Program, 160, pp. 723–782.
Robertson, A.H.F., 2002. Overview of the genesis and emplacement of Mesozoic ophiolites in the Eastern Mediterranean Tethyan region. Lithos 65, 10–67.
Robertson, A.H.F., Mountrakis, D., 2006. Tectonic development of the Eastern Mediterranean region: an introduction. Geological Society of London, Special Publication 260, 1–9.
Santosh, M., Maruyama, S., Sato, K., 2009. Anatomy of a Cambrian suture in Gondwana: Pacific-type orogeny in southern India? Gondwana Research 16, 321–341.
Sengor, A.M.C., 1990. A New Model for the late Paleozoic–Mesozoic Tectonic Evolution of Iran and Implications for Oman. In: Robertson, A.H.F., Searle, M.P., Ries, A.C. (Eds.), The Geology and Tectonics of the Oman Region: Geological Society Special Publication, 49, pp. 797–831.
Shafaii Moghadam, H., 2009. The Nain-Baft Ophiolites (Central Iran): Age, Structure and Origin [Ph.D. thesis]: Tehran, Iran, Shahid Beheshti University, 532pp.
Shafaii Moghadam, H., Stern, R.J., 2011. Geodynamic evolution of upper Cretaceous Zagros ophiolites: formation of oceanic lithosphere above a nascent subduction zone. Geological Magazine 148, 762–801.
Shafaii Moghadam, H., Whitechurch, H., Rahgoshay, M., Monsef, I., 2009. Significance of Nain-Baft ophiolitic belt (Iran): short-lived, transtensional Cretaceous back-arc oceanic basins over the Tethyan subduction zone. Comptes Rendus Geosciences 341, 1016–1028.
Shafaii Moghadam, H., Stern, R.J., Rahgoshay, M., 2010. The Dehshir ophiolite (Central Iran): geochemical constraints on the origin and evolution of the Inner Zagros Ophiolitic Belt. Geological Society of America Bulletin 122, 1516–1547.
Shafaii Moghadam, H., Stern, R.J., Kimura, J.A., Hirahara, Y., Senda, R., Miyazaki, T., 2012a. Hf–Nd isotope constraints on the origin of Dehshir Ophiolite, Central Iran. Island Arc 21, 202–214.
Shafaii Moghadam, H., Mosaddegh, H., Santosh, M., 2012b. Geochemistry and petrogenesis of the Late Cretaceous Haji-Abad ophiolite (Outer Zagros Ophiolite Belt, Iran): implications for geodynamics of the Bitlis–Zagros suture zone. Geological Journal. http://dx.doi.org/10.1002/gj.2458.
Shafaii Moghadam, H., Corfu, F., Stern, R.J., 2013. U-Pb Zircon ages of Late Cretaceous Nain-Dehshir ophiolite, Central Iran. Journal of the Geological Society of London 170, 175–184.
Shahabpour, J., 2005. Tectonic evolution of the orogenic belt in the region located between Kerman and Neyriz. Journal of Asian Earth Sciences 24, 405–417.
Shervais, J.W., 1982. Ti-V plots and the petrogenesis of modern ophiolitic lavas. Earth and Planetary Science Letters 59, 101–118.
Shervais, J.W., 2001. Birth, death and reconstruction: the life cycle of suprasubduction zone ophiolites. Geochemistry, Geophysics, Geosystems 2 (2000GC000080).
Srdic, A., Dimitrijevic, M.N., Cvetic, S., Dimitrijevic, M.D., 1972. Geological map of Baft, 1/100000 Series, Sheet 7348, Geological Survey of Iran.
Stakes, D.S., Franklin, J.M., 1994. Petrology of Igneous Rocks at Middle Valley, Juan de Fuca Ridge. In: Mottl, M.J., Davis, E.E., Fisher, A.T., et al. (Eds.), Proceedings of the Ocean Drilling Program, Scientific Results, 139, College Station, Texas, pp. 79–102.
Stern, R.J., 2002. Subduction zones. Reviews of Geophysics 40 (4), 1012. http://dx.doi.org/10.1029/2001RG000108.
Stern, R.J., 2004. Subduction initiation: spontaneous and induced. Earth & Planetary Science Letters 226, 275–292.
Stern, R.J., 2010. The anatomy and ontogeny of modern intra-oceanic arc systems. In: Kusky, T.M., Zhai, M.G., Xiao, W. (Eds.), The Evolving Continents: Understanding Processes of Continental Growth: Geological Society of London, Special Publication, 338, pp. 7–34.
Stern, R.J., Bloomer, S.H., 1992. Subduction zone infancy; examples from the Eocene Izu-Bonin–Mariana and Jurassic California arcs. Geological Society of America Bulletin 104, 1621–1636.
Stocklin, J., 1977. Structural correlation of the Alpine range between Iran and Central Asia. Memoire Hors-Serve No.8. Societé Geologie de la France 8, 333–353.
Stocklin, J., Eftekhar-Nezhad, J., Hushmandzadeh, A., 1972. Central Lut Reconnaissance, East Iran. Geological Survey of Iran, report No.22.
Sun, S.S., McDonough, W.F., 1989. Chemical and isotopic systematics of oceanic basalts: implications for mantle composition and processes. In: Saunders, A.D., Norry, M.J. (Eds.), Magmatism in Ocean Basins: Geol. Soc. Spec. Publ., London, pp. 313–345.
Tamura, A., Arai, S., 2006. Harzburgite–dunite–orthopyroxenite suite as a record of supra-subduction zone setting for the Oman ophiolite mantle. Lithos 90, 43–56.
Tatsumi, Y., Hamilton, D.L., Nesbitt, R.W., 1986. Chemical characteristics of fluid phase related from a subducted lithosphere and origin of arc magmas: evidence from high pressure experiments and natural rocks. Journal of Volcanology and Geothermal Research 29, 293–309.
Tsuchiya, N., Shibata, T., Yoshikawa, M., Adachi, Y., Miyashita, S., Adachi, T., Nakano, N., Osanai, Y., 2013. Petrology of Lasail plutonic complex, northern Oman ophiolite, Oman: an example of arc-like magmatism associated with ophiolite detachment. Lithos 159, 120–138.
VanderLaan, S.R., Arculus, R.J., Pearce, J.A., Murton, B.J., 1992. Petrography, Mineral Chemistry, and Phase Relations of the Basement Boninite Series of site 786, Izu-Bonin Forearc. In: Fryer, P., Pearce, J.A., Stokking, L.B., et al. (Eds.), Proceedings of the Ocean Drilling Program, Scientific Results, 125, College Station, Texas, pp. 171–201.
Warren, C.J., Parrish, R.R., Waters, D.J., Searle, M.P., 2005. Dating the geologic history of Oman's Semail ophiolite: insights from U–Pb geochronology. Contributions to Mineralogy and Petrology 150, 403–422.
Whattam, S.A., Stern, R.J., 2011. The 'subduction initiation rule': a key for linking ophiolites, intra-oceanic forearcs, and subduction initiation. Contributions to Mineralogy and Petrology. http://dx.doi.org/10.1007/s00410-011-0638-z.
Yaliniz, K.M., Floyd, P., Goncuoglu, M.C., 1996. Supra-subduction zone ophiolites of central Anatolia: geochemical evidence from the Sarikaraman ophiolite, Aksaray, Turkey. Mineralogical Magazine 60, 697–710.
Yellappa, T., Santosh, M., Chetty, T.R.K., Kwon, S., Park, C., Nagesh, P., Mohanty, D.P., Venkatasivappa, V., 2011. A Neoarchean dismembered ophiolite complex from southern India: Geochemical and geochronological constraints on its suprasubduction origin. Gondwana Research. http://dx.doi.org/10.1016/j.gr.2011.05.003.